# Validation of the suitability of mouse neuroblastoma cells in the study of chloride homeostasis using patch-clamp

Master's Thesis
Anna-Sofia Mäkitiura
Degree Programme in Physics
Faculty of Science
University of Oulu
2023

## Abstract

The function of the nervous system is dependent on the balance between excitatory and inhibitory activity. In the central nervous system (CNS), the homeostasis of $Cl^-$ is in a key role in modulating neuronal excitability, since the intracellular $Cl^-$ concentration ($[Cl^-]_i$) determines the postsynaptic responses mediated by GABA and glycine, the main inhibitory neurotransmitters. Deficiency in the regulation of $Cl^-$ homeostasis, that is maintained by various ion channels and transporters, is associated with many neurological disorders such as epilepsy. Hence, the understanding of the mechanisms underlying the regulation of $Cl^-$ homeostasis is important.

Patch-clamp is an electrophysiological method that is used to study the electrical properties of excitable cells. It is a versatile technique, as it provides information of the concentration gradients of ions as well as ion channel kinetics. One important electrophysiological parameter describing channel function is the reversal potential of an ion $i$ ($E_i$). Patch-clamp experiments can be done by using cultured cells or tissue slices, which can be genetically modified to express exogenous proteins, such as membrane transporters. There are a variety of cell lines that can be used as expression systems in patch-clamp, such as the commercial mouse neuroblastoma (N2a) cell line, that is used in the experiments in this thesis.

The aim of this thesis is to validate the suitability of the N2a cell line as an expression system for $E_{Cl}$ recordings using patch-clamp. In the experiments, whole-cell configuration of the patch-clamp was used to study the endogenous voltage-gated currents that are expressed in the N2a cell line, especially in the voltage-range wherein the $E_{Cl}$ typically lies.

## List of abbreviations

| Abbreviation | Definition | Unit |
|---|---|---|
| $K^+$ | Potassium ion | |
| $Na^+$ | Sodium ion | |
| $Cl^-$ | Chloride ion | |
| $Ca^{2+}$ | Calcium ion | |
| $[C]$ | Concentration of an ion | mol/l (M) |
| ATP | Adenosine triphosphate | |
| GABA | Gamma-aminobutyric acid | |
| CNS | Central nervous system | |
| PSC | Postsynaptic current | |
| PSP | Postsynaptic potential | |
| CCC | Cation-chloride cotransporter | |
| NKCC1 | $Na^+$-$K^+$-$2Cl^-$-cotransporter type 1 | |
| KCC2 | $K^+$-$Cl^-$-cotransporter type 2 | |
| N2a | Neuroblastoma cell line | |
| $V_m$ | Membrane potential | mV |
| $R_m$ | Membrane resistance | Ω |
| $C_m$ | Membrane capacitance | pF |
| $I_m$ | Membrane current | pA |
| $E_i$ | Nernst potential of an ion | mV |
| I-V relation | Current-voltage relation | |
| TTX | Tetrodotoxin | |
| TEA | Tetraethylammonium | |
| LJP | Liquid junction potential | mV |
| $R_e$ | Electrode resistance | MΩ |
| $V_c$ | Command voltage | mV |
| $R_s$ | Series resistance | MΩ |
| $\Delta V$ | Voltage-error due to series resistance | mV |
| ClC | Voltage-gated chloride channel | |
| GlyR | Glycine receptor | |
| GPPC | Gramicidin perforated patch-clamp | |
| CHO | Chinese hamster ovary cell line | |
| HEK293 | Human embryonic kindey cell line | |
| Kv channel | Voltage-gated potassium channel | |
| Nav channel | Voltage-gated sodium channel | |
| *Eag* | *Ether-á-go-go* | |
| *Erg* | *Ether-á-go-go*-related gene | |
| $V_{1/2}$ | Half-activation potential | mV |
| $k$ | Slope factor | |

# Contents

# 1 Introduction

Neurons, along with other excitable cells, are specialized in conducting information in the form of electrical signals. These electrical signals, propagated as action potentials via the axon of the cell, are a result of transmembrane ion currents. The major ion species contributing to these currents in the nervous system are potassium ($K^+$), sodium ($Na^+$), chloride ($Cl^-$) and calcium ($Ca^{2+}$). In the membranes of neurons, there are a variety of transmembrane proteins capable of transporting ions, which include active and passive membrane transporters. [1]

Ion pumps, such as $Na^+$-$K^+$-ATPase, are primary active transporters, which transport ions against their concentration gradients. Ion pumps derive their energy from the hydrolysis of adenosine triphosphate (ATP). They create and maintain the electrochemical gradient that is utilized to the transport of ions by ion channels. [1]

Ion channels are selectively permeable to specific ions, that can cross the membrane through a channel pore. Ion channels can be classified by gating, meaning what affects their open or closed state, or by the type of ions they transport. The main types of gated ion channels are voltage-gated and ligand-gated ion channels. The open and closed state of voltage-gated ion channels is dependent on the voltage gradient across the membrane, whereas that of the ligand-gated channels is dependent on binding of ligands, such as neurotransmitters, to the extracellular domain of the receptor protein. The membrane potential is determined by the permeability and concentrations of specific ions between the intracellular and extracellular spaces and it changes in response to any changes in its environment. There are also ion channels that switch between open and closed state without gating, which are referred to as leak channels. However, the opening of the leak channels can be modulated by changing pH, temperature or with specific molecules, for example. [1, 2, 3]

Another group of membrane transporters are secondary active ion cotransporters. They are able to carry ions and molecules against their concentration gradient using the electrochemical gradient of other ions. Hence, the transport is based on an indirect use of the energy from the hydrolysis of ATP. Cotransporters can be classified to antiporters, which are also called ion exchangers, and symporters. Antiporters move the ions or molecules in opposite directions, while symporters move them in the same direction. [1]

The communication between neurons is provided by synapses, that can be classified to electrical and chemical synapses. Electrical synapses allow direct, passive flow of ions through gap junctions from one neuron to another. At chemical synapses, electrical activity in the presynaptic neuron results in the release of neurotransmitters that further bind to receptors located in the membrane of the postsynaptic neuron. Chemical synapses can be classified according to the neurotransmitters they release, such as glutamatergic and GABAergic synapses. Glutamate is the most abundant excitatory neurotransmitter, whereas gamma-aminobutyric acid (GABA), along with glycine, is the main inhibitory neurotransmitter in mature central nervous system (CNS). [1, 2]

Binding of neurotransmitters to postsynaptic receptors changes the postsynaptic conductance, due to the activation of ion channels of the postsynaptic membrane. The postsynaptic conductance increases when channels open and decreases when channels close. The conductance change typically creates a postsynaptic current (PSC), which further changes the postsynaptic membrane potential, producing a postsynaptic potential (PSP). PSPs are excitatory (EPSP) when they increase the probability of an action potential and inhibitory (IPSP) when they decrease the probability of an action potential occurring. [3]

In order to function normally, there must be both excitatory and inhibitory action in the ner-

vous system. The fast inhibitory synaptic transmission mediated by GABA and glycine is highly dependent on the gradient of $Cl^-$. The members of secondary active *Slc12a* family of cation-chloride cotransporters (CCCs) are the primary regulators of the neuronal $Cl^-$ gradient. The $Na^+$-$K^+$-$2Cl^-$ cotransporter type 1 (NKCC1) is the major $Cl^-$ transporter during early development. NKCC1 transports $Cl^-$ into the neuron, maintaining a relatively high intracellular $Cl^-$ concentration ($[Cl^-]_i$). [4, 5]

In mature neurons, a neuron-specific member of the CCC family, $K^+$-$Cl^-$ cotransporter type 2 (KCC2) uses the energy of $K^+$ gradient to transport $Cl^-$ out of neurons, therefore maintaining a low $[Cl^-]_i$. Activation of the $GABA_A$ receptor ($GABA_AR$) results in an inward $Cl^-$ current, which hyperpolarizes the membrane. Deficiency or absence of KCC2 results in an increase of $[Cl^-]_i$, which in turn decreases the inhibitory effect of GABA and glycine. Furthermore, KCC2 deficiency compromises the formation and maturation of inhibitory synaptic connections, resulting in hyperexcitability and seizure activity, which is typical in some neural disorders, such as epilepsy and schizophrenia. [3, 4, 5]

There are a variety of methods that have been used to study $Cl^-$ homeostasis, such as the patch-clamp method used in electrophysiology. The aim of this thesis is to study the endogenous, voltage-sensitive currents in the mouse neuroblastoma (N2a) cells with the patch-clamp method and to validate the use of these cells to study $Cl^-$ homeostasis.

# 2 Review of literature

## 2.1 Excitable cells

Cells are the fundamental units of all living organisms. Excitable cells, such as neurons, are specialized in conducting information in the form of electrical signals propagated as action potentials. There is a great variety of different types of neurons that can be morphologically and functionally distinguished in the nervous system. However, the main structures are similar. A schematic of a generic multipolar neuron and a chemical synapse are shown in Figure 1. [1, 2]

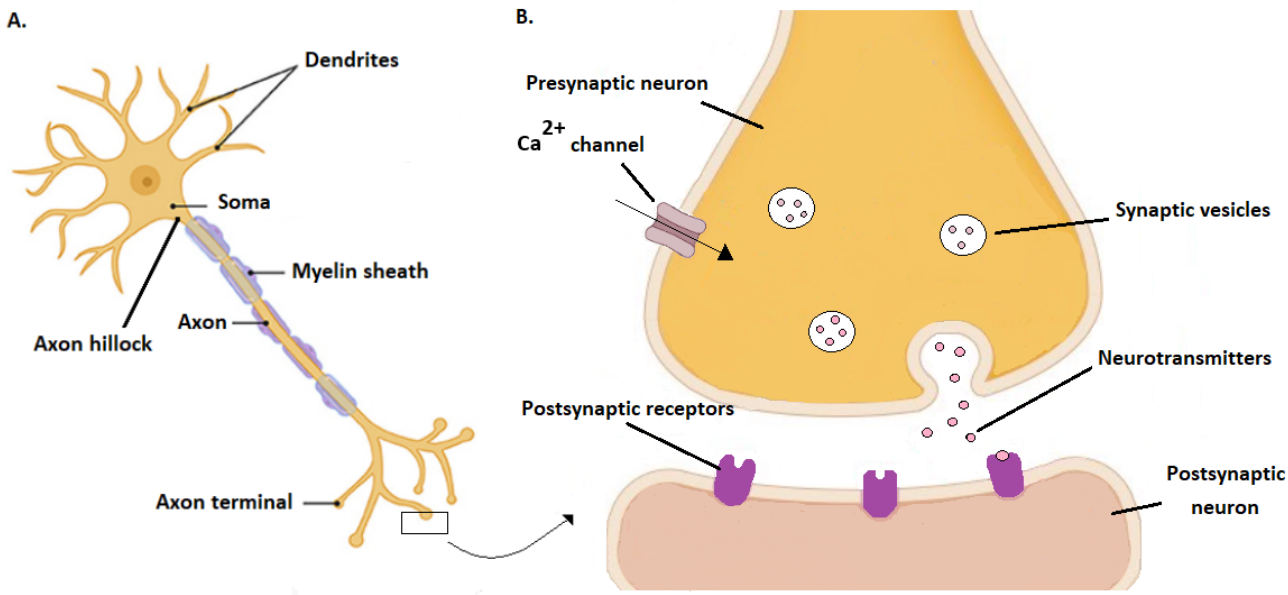


Figure 1: *A*. Multipolar neuron with myelin sheath. *B*. Chemical synapse. As an action potential reaches the presynaptic terminal, it depolarizes the membrane. As a result, voltage-gated $Ca^{2+}$ channels open, which further causes the neurotransmitter-carrying vesicles to fuse with the presynaptic membrane. Figure 1 *A* modified from Doblado L. R., Martinez-Ramos C., Pradas M. M., Biomaterials for Neural Tissue Engineering, Frontiers in Nanotechnology, Vol 3 (2021) *https://www.frontiersin.org/articles/10.3389/fnano.2021.643507/full.*

Neurons are eukaryotic cells, which are delineated by the cell membrane, that is a lipid bilayer, mainly consisting of phospholipids and cholesterols. There are various membrane proteins embedded in the cell membrane, such as transport proteins. Cell body, also known as the soma, contains the cell nucleus, in which the genetic information is stored, and other organelles, such as the endoplasmic reticulum, mitochondria and ribosomes. [1, 2]

Axon is an extension of the neuron, in which the signal travels to another neuron, and it is connected to the soma by the axon hillock. Action potential propagates to the axon terminal, that is also referred to as the presynaptic terminal. Some axons are surrounded by myelin sheath, that acts as an insulating substance. Gaps in the myelin sheath are called nodes of Ranvier, in which an action potential is regenerated. In the CNS, myelin is produced by a special type of glial cells, oligodendrocytes, whereas in the peripheral nervous system (PNS) Schwann cells are responsible

for that. Myelin reduces transmembrane resistive and capacitive currents in the internodal region, enabling faster transmission of information. This type of electrical impulse propagation is called saltatory conduction. [1, 2]

The pathway connecting a presynaptic terminal to its postsynaptic target cell is referred to as a synapse. Chemical synapses are the most abundant type of synapse in the nervous system. The connection between two cells in a chemical synapse is a synaptic cleft, whereas that of an electrical synapse is referred to as a gap junction. Dendrites of neurons are the primary target for synaptic input, in which the information is transmitted to the soma of the postsynaptic cell. Dendrites have a high content of ribosomes and specific cytoskeletal proteins. [1, 2]

Synaptic vesicles are lipid bilayer sacs filled with cytosolic fluid and neurotransmitters, which function as the secretory organelles in the presynaptic terminals of chemical synapses. As an action potential reaches a presynaptic neuron, the membrane becomes depolarized, which leads to the opening of voltage-gated $Ca^{2+}$ channels. As a result of an influx of $Ca^{2+}$, synaptic vesicles fuse with the membrane and neurotransmitters are released to the synaptic cleft. As they bind to specific receptors of the target cells, neurotransmitters induce a change in the membrane potential of the postsynaptic cell. [1, 2]

Membrane transport proteins, including ion channels and ion transporters, are responsible for the movement of ions across the membranes of neurons. Therefore, they are in a key role in maintaining the cellular homeostasis. In cells, homeostasis refers to internal conditions that are maintained within a stable range despite any changes in the environment. All cells must maintain homeostasis in order to function normally. The mechanisms requiring energy within a cell are said to be in steady state, or dynamic equilibrium. [1]

There are a variety of techniques to study the function of membrane transporters and ion movement. These techniques are usually based on electrophysiology. In the next section, the fundamental physical laws concerning the electrophysiological properties of excitable cells are discussed in more detail.

## 2.2 Biophysics of the cell membrane

Some of the membrane proteins act as membrane transporters, regulating the movement of different substances across the membrane via passive and active transport. The passive flow of ions from high concentration to low concentration is referred to as diffusion. Since ions are charged particles, their movement is influenced by their concentration gradient as well as their electric field. The movement of ions due to their concentration gradients can be described with Fick's diffusion law, which is determined as

$$J_{diff} = -D\frac{d[C]}{dx}, \tag{1}$$

where $J$ is diffusion flux ($molecules/s \cdot cm^2$), $D$ is the diffusion coefficient ($cm^2/s$) and [C] is the ion concentration ($mol/cm^3$). Diffusion goes down the concentration gradient, which is indicated by the negative sign. Diffusion is also directly proportional to the magnitude of the gradient in terms of the diffusion coefficient $D$. [1]

The interaction between electric charges of ions, and the electric field surrounding them, results in a force experienced by the ions. Ohm's law for drift describes the flow of charged particles taking that interaction into account, which can be described with equation

$$J_{drift} = d_{el}E = -\mu z[C]\frac{dV}{dx}, \tag{2}$$

where $J_{drift}$ is the drift flux ($molecules/s \cdot cm^2$), $d_{el}$ is electrical conductivity ($molecules/V \cdot s \cdot cm$), $E$ is electric field ($V/cm$), $V$ is electric potential ($V$), $\mu$ is mobility ($cm^2/Vs$), $z$ is the valence of an ion and [C] is the concentration. The equation indicates that drift for positively charged particles goes down the electric potential gradient and that it is directly proportional to the magnitude of the gradient. [1]

The total ion flux, resulting from both the concentration gradient and electric field, can be determined by combining the diffusion and drift flux:

$$J = J_{drift} + J_{diff} = -\mu z[C]\frac{dV}{dx} - D\frac{d[C]}{dx}. \tag{3}$$

The relation between diffusion and drift was shown by Einstein (1905), stating that the two processes experience the same frictional resistances in the same medium. By the Einstein relation, diffusion coefficient and mobility are related by

$$D = \frac{kT}{q}\mu, \tag{4}$$

where $k$ is Boltzmann's constant ($1.381 \cdot 10^{-23}$ J/K), $T$ is temperature in Kelvin and $q$ is the charge. [1]

The law of space-charge neutrality states that in a given volume, the total charges of cations is approximately equal to the total charges of anions. The law of space-charge neutrality holds everywhere in a biological system except for the cell membrane, since the electric field is nonzero across it. This condition can be described by Gauss's law, which states that the electric field at the surface of a given volume is proportional to the total charge within that volume. This can be expressed as

$$\int \mathbf{E} d\mathbf{a} = 4\pi \int \rho dv = 4\pi q, \tag{5}$$

where $\mathbf{E}$ is the electric field, $\mathbf{a}$ is the area, $\rho$ is the charge density, $v$ is the volume and $q$ is the total charge. [1]

Using the Einstein relation, the diffusion coefficient can be expressed in terms of mobility, which gives the Nernst-Planck equation of the ion flux:

$$J = -\left(\mu z[C]\frac{dV}{dx} + \frac{\mu kT}{q}\frac{d[C]}{dx}\right). \tag{6}$$

The Nernst-Planck equation describes the passive ion currents mediated by electrochemical potentials, or the sum of concentration gradient and electric field. [1]

The Nernst-Planck equation in molar form is obtained by dividing the flux $J$ by Avogadro's number ($N_A = 6.022 \cdot 10^{23} 1/mol$), which can be expressed as

$$J = J/N_A = \frac{-\mu z[C]}{N_A}\frac{dV}{dx} - \frac{\mu kT}{N_A q}\frac{d[C]}{dx} = -\left(uz[C]\frac{dV}{dx} + u\frac{RT}{F}\frac{d[C]}{dx}\right), \tag{7}$$

where $u$ is the molar mobility ($\mu/N_A$ expressed as $cm^2/V \cdot s \cdot mol$) and $R$ is the gas constant ($8.314 J/K \cdot mol$). [1]

### 2.2.1 Nernst equation

Current is the product of ion flux and the charge carried by the flux. Therefore, the current density form of the Nernst-Planck equation can be expressed as

$$I = \mathbf{J} \cdot zF = -\left(uz^2F[C]\frac{dV}{dx} + uzRT\frac{d[C]}{dx}\right). \tag{8}$$

When the cell membrane is at rest, the net current is zero. Thus, the resting membrane potential can be derived from the Nernst-Planck equation by setting the equation (8) equal to zero:

$$I = -\left(uz^2F[C]\frac{dV}{dx} + uzRT\frac{d[C]}{dx}\right) = 0$$

For $\frac{dV}{dx}$,

$$\frac{dV}{dx} = \frac{-RT}{zF}\frac{1}{[C]}\frac{d[C]}{dx}$$

Integrating in terms of membrane potential and concentration yields

$$\int_{V1}^{V2} dV = -\frac{RT}{zF}\int_{[C_1]}^{[C_2]}\frac{d[C]}{[C]} \rightarrow V_2 - V_1 = -\frac{RT}{zF}ln\frac{[C_2]}{[C_1]}. \tag{9}$$

Defining the membrane potential as $V_m = V_{in} - V_{out}$, the equilibrium potential of ion $i$ can be defined as

$$E_i = V_{in} - V_{out} = \frac{RT}{zF}ln\frac{[C_i]_{out}}{[C_i]_{in}}, \tag{10}$$

The equation (10) is called the Nernst equation and it determines the membrane potential at which the membrane current carried by ion $i$ is zero, which is called the Nernst potential ($E_i$). The Nernst equation implies that when the membrane potential equals the equilibrium potential of an ion, the concentration gradient and the membrane voltage cancel each other. The ionic concentration gradient across the membrane allows the movement of the ions. That drives ion flow according to the laws of diffusion and drift. [1]

When a cell is at rest, most of its gated channels are closed. Thus, the movement of ions at rest is mostly mediated by spontaneous leak channels. The leak currents typically include outward flow of potassium and little influx of sodium, since most membranes are more permeable to potassium and chloride than to sodium. [1]

Permeability describes the rate of passive diffusion and ion selectivity. It can be determined empirically by

$$J = -P\Delta[C], \tag{11}$$

where $J$ is the molar flux and $P$ is membrane permeability to an ion ($cm/s$). When assuming [C] to linearly change with respect to $x$, it can be given as

$$\frac{d[C]}{dx} = \frac{\Delta[C]\beta}{l}, \tag{12}$$

where $\beta$ is the water-membrane partition coefficient and $l$ is the thickness of the membrane. Given this, the ion permeability can be expressed as

$$P = \frac{D\beta}{l}. \tag{13}$$

### 2.2.2 Equivalent circuit model

The cell membrane acts as an insulator. In contrast, both the extracellular and the intracellular sides of the membrane consist of conductive saline solution. Therefore, the cell membrane is considered a parallel-plate capacitor. Capacitance is dependent on the dielectric constant of the medium as well as the geometry of the conductors. The capacitance of a capacitor of two parallel plates can be determined by

$$C = \frac{\varepsilon\varepsilon_0 A}{d}, \tag{14}$$

where $\varepsilon$ is the dielectric constant of the insulator and $\varepsilon_0$ is the vacuum permittivity ($8.85 \cdot 10^{-12} C/Vm$), $A$ is the area of the plates of the insulator and $d$ is the distance between the plates. The capacitance per square centimetre, or the specific membrane capacitance of biological membranes, is typically 1 $\mu F/cm^2$. [1, 3]

A capacitor can store charge proportionally to the applied voltage, according to the equation

$$Q = CV, \tag{15}$$

where $Q$ is charge, $C$ is capacitance and $V$ is voltage. Current is determined by the rate of flow of charge, that can be expressed as

$$I = \frac{dQ}{dt}. \tag{16}$$

Thus, differentiation of the equation (15) yields

$$I = C\frac{dV}{dt}. \tag{17}$$

The equation (17) implies that there must be current flow in order to change the membrane potential. On the other hand, a capacitor prevents instantaneous changes of voltage across it. [1, 3]

The membrane resistance ($R_m$) is reciprocal to the membrane conductance ($G_m$). Both of these describe ion permeation through ion channels and are highly dependent on both voltage and time. The current flow in a resistor follows Ohm's law, that is defined by

$$V = RI. \tag{18}$$

The electrical properties of the cell membrane and ion channels are typically represented by electrical circuit diagrams that are referred to as equivalent circuits. An equivalent circuit model of a cell expressing $Na^+$, $K^+$ and $Cl^-$ channels is shown in Figure 2. The equivalent circuit model describes the cell as a capacitor with membrane capacitance $C_m$ connected in parallel with ion channels. [1, 3]

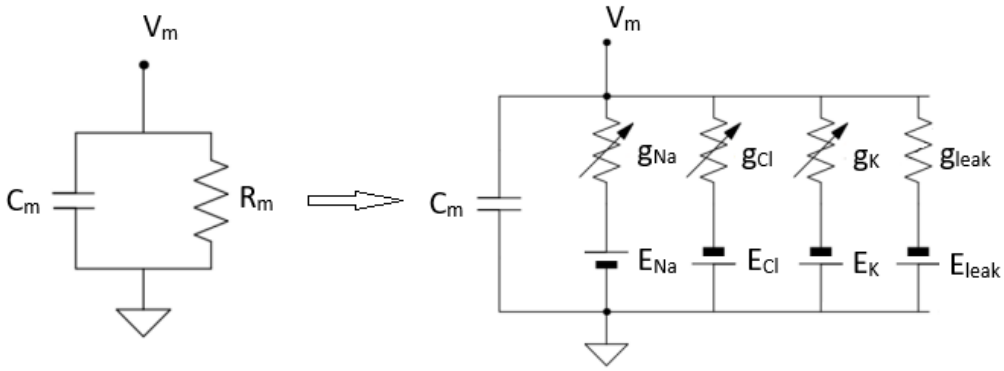


Figure 2: The equivalent circuit model of a one-compartment cell with membrane capacitance $C_m$, expressing $Na^+$, $K^+$ and $Cl^-$ channels. $C_m$ is the membrane capacitance, $V_m$ is the membrane potential and $R_m$ is the membrane resistance. $E_{Na}$, $E_{Cl}$, and $E_K$ are the reversal potentials of $Na^+$, $K^+$ and $Cl^-$, respectively and $g_{Na}$, $g_{Cl}$, and $g_K$ are the conductances of $Na^+$, $K^+$ and $Cl^-$, respectively.

According to the equivalent circuit representation, Kirchhoff's current law and Ohm's law, the differential equation for the total current flow across the membrane ($I_m$) can be given as

$$I_m = I_c + I_i = C_m \frac{dV_m}{dt} + \frac{(V_m - E_r)}{R_m} = C_m \frac{dV_m}{dt} + G_m(V_m - E_r) \tag{19}$$

where $I_c$ is the capacitive current, $I_i$ the ionic current, $C_m$ is the specific membrane capacitance ($F/cm^2$), $R_m$ is the specific membrane resistance ($\Omega \cdot cm^2$), $G_m$ is the specific membrane conductance ($S/cm^2$) and $(V_m - E_r)$ is the driving force of ionic current. The driving force is the difference between the membrane potential and the reversal potential of the cell. [1, 3]

The total ionic current $I_i$ can be separated to the currents carried by individual ions, i.e., $I_i = I_{Na} + I_K + I_{Cl}$. Furthermore, the membrane current can be given in terms of membrane conductance, which is given as

$$I_m = C_m \frac{dV}{dt} + g_K(V_m - E_K) + g_{Na}(V_m - E_{Na}) + g_{Cl}(V_m - E_{Cl}) \tag{20}$$

which is the parallel conductance model. It can be used to describe the steady state potential, at which the cell is at rest and the net current is zero. In this case, since the current is zero, there is no capacitive current. Therefore, the steady state potential can be described with equation

$$V_m = \frac{g_K E_K + g_{Na} E_{Na} + g_{Cl} E_{Cl}}{g_K + g_{Na} + g_{Cl}}. \tag{21}$$

In case the conditions within the membrane can be described with Nernst-Planck equation and when the electric field of the membrane is constant, it can be described with Goldman-Hodgkin-Katz (GHK) constant field model. [1]

### 2.2.3 Constant field model

In order to use the constant field model, ion movement within the membrane must obey the Nernst-Plank equation and the ions must move without interacting with other ions. Furthermore the electric field has to be constant, which can be expressed as

$$E = -\frac{dV}{dx} = -\frac{V}{l}. \tag{22}$$

In this case, the current across the membrane can be determined by the Nernst-Planck equation:

$$I = uz^2 F[C]\frac{dV}{dx} + uzRT\frac{d[C]}{dx}. \tag{23}$$

When current flows from inside of the cell to outside of the cell, it is defined to be positive. Defining

$$y = I - \frac{uz^2 F[C]V}{l}$$

Then

$$\frac{dy}{dx} = \frac{dI}{dx} - \frac{uz^2 FV}{l}\frac{d[C]}{dx}, \tag{24}$$

and in steady state $\frac{dI}{dx} = 0$.
Substituting equation (23) into the equation (24), gives

$$y = uz^2 F[C]\frac{V}{l} - uzRT\frac{d[C]}{dx} - \frac{uz^2 F[C]V}{l} = \frac{RTl}{zFV}\frac{dy}{dx}. \tag{25}$$

Integrating the equation (25) yields

$$\int_{x=0}^{x=l} dx = \frac{RTl}{zFV}\int_{y(C_{x=l})}^{y(C_{x=0})} \frac{dy}{y}.$$

Now for $l$

$$l = \frac{RTl}{zFV} ln \frac{I - \frac{uz^2FV\beta}{l}[C]_{out}}{I - \frac{uz^2FV\beta}{l}[C]_{in}}. \tag{26}$$

In terms of $I$

$$I = \frac{uz^2FV\beta}{l} \left( \frac{[C]_{out} e^{\frac{-zFV}{RT}} - [C]_{in}}{e^{\frac{-zFV}{RT}} - 1} \right) \tag{27}$$

which can be expressed as

$$I = PzF\xi \left( \frac{[C]_{in} - [C]_{out} e^{-\xi}}{1 - e^{-\xi}} \right). \tag{28}$$

The current-voltage relation (I-V relation) of a cell or ionic current is given by the GHK current equation. It can be divided into two independent equations describing the outward flux and the inward flux:

$$I_{out} = PzF\xi \frac{[C]_{in}}{1 - e^{-\xi}} \tag{29}$$

and

$$I_{in} = -PzF\xi \frac{[C]_{out} e^{-\xi}}{1 - e^{-\xi}}. \tag{30}$$

The GHK current equation is a nonlinear function. In the next section, current-voltage relation is discussed more in detail. However, the membrane conductance typically changes with changing voltage. This property is referred to as rectification and it is dependent on the ratio of ion concentrations. When $[C]_{out} = [C]_{in}$, the IV relation is linear. Otherwise, it shows either outward rectification (when $[C]_{out} < [C]_{in}$) or inward rectification ($[C]_{out} > [C]_{in}$).

The total current can be separated in case the cell is permeable to multiple ions, for example as follows

$$\begin{aligned} I &= I_K + I_{Na} + I_{Cl} \\ &= P_K zF\xi \frac{[K^+]_{in} - [K^+]_{out} e^{-\xi}}{1 - e^{-\xi}} + P_{Na} zF\xi \frac{[Na^+]_{in} - [Na^+]_{out} e^{-\xi}}{1 - e^{-\xi}} + P_{Cl} zF\xi \frac{[Cl^-]_{in} - [Cl^-]_{out} e^{-\xi}}{1 - e^{-\xi}}. \end{aligned} \tag{31}$$

The GHK voltage equation describes the steady state membrane potential or the resting membrane potential. At steady state, $I = 0$, and the corresponding voltage can be given as

$$V = \frac{RT}{F} ln \frac{P_K[K^+]_{out} + P_{Na}[Na^+]_{out} + P_{Cl}[Cl^-]_{in}}{P_K[K^+]_{in} + P_{Na}[Na^+]_{in} + P_{Cl}[Cl^-]_{out}}, \tag{32}$$

The equation (32) is called the GHK voltage equation. The equation is very useful in describing the behaviour of the cell membrane. For example, previously mentioned resting membrane potential can be described with it as well as the action potential, whenever the permeabilities of the ions are known. [1]

## 2.3 Voltage-clamp

Voltage-clamp is a technique used in electrophysiology, which allows the study of electrical properties of excitable cells. In voltage-clamp, the membrane voltage is recorded and compared to the command voltage. With the use of negative feedback, current is injected to set the voltage difference at zero, which clamps the membrane voltage to a desired value. Therefore, the resulting membrane currents can be recorded at each voltage. [1, 2]

The history of voltage-clamp started around the 1940s. There is uncertainty of who first had the idea of voltage-clamp, but Kenneth Cole and George Marmont used the technique back in 1947. Alan Hodgkin and Andrew Huxley had independently discussed the idea as well. However, Hodgkin and Huxley continued studies and developed their dual electrode technique, which allowed them to record the ionic currents across the axonal membrane of a squid giant axon without any significant change in membrane potential. They improved the technique, so that electrode polarization could be avoided. They later described how ionic currents generate the action potential. Eventually, Hodgkin and Huxley shared the Nobel Prize in Physiology or Medicine in 1963. [1, 2, 7]

The voltage-clamp experiments of the squid giant axon showed that the membrane current consists of a fast, early inward current mediated by $Na^+$, followed by a slowly activating outward current mediated by $K^+$. The currents can be separated, which proves this result. For example, removing the extracellular $Na^+$ eliminates the driving force of the inward $Na^+$ flux, and as a result, the $K^+$ current is left. The same result is seen when adding tetrodotoxin (TTX) in the solution, since it blocks the $Na^+$ channels from activating. In contrast, if eliminating the potassium current, only the current mediated by $Na^+$ channels can be seen. This can be done by removing the intracellular $K^+$, which eliminates the driving force of the efflux of $K^+$, or by the use of tetraethylammonium (TEA) for example, which acts as a blocker of $K^+$ channels. [1]

When it comes to the gating kinetics of ion channels, previously defined with equation (20), Hodgkin and Huxley came up with an even more precise model, including specific gating variables $n$, $m$ and $h$, which define the proportional conductance for $K^+$ and $Na^+$ at a given time and voltage. This model can be shown as

$$I = C_m \frac{dV}{dt} + \bar{g}_k n^4 (V - V_K) + \bar{g}_{Na} m^3 h (V - V_{Na}) + \bar{g}_l (V - V_l). \tag{33}$$

Overall, the methods and mathematical models created by Hodgkin and Huxley have been the foundations for many other electrophysiologists, leading to a growing interest in the field of electrophysiology. [7]

A special technique developed from voltage-clamp is the patch-clamp method, which was developed by Erwin Neher and Bert Sakmann in the 1970s. Compared to voltage-clamp, patch-clamp is done using a single electrode within a glass micropipette, which allowed the study of single ion channels of small cells. The same electrode not only records the membrane potential but is also used to inject current. The pipette forms a high-resistance seal with the membrane, which is referred to as a gigaseal and allows the low-noise recording of tiny, picoampere level signals. Neher and Sakmann were awarded with the Nobel Prize in Physiology or Medicine in 1991 for their discoveries concerning the functioning of single ion channels. [6, 7]

Patch-clamp can be used in various configurations, such as in whole-cell configuration or cell-attached configuration. Furthermore, perforated patch-clamp is a technique in which a pore-forming agent is used. The equipment and theory involved in patch-clamp are discussed in more detail in the following section. [8, 9]

## 2.4 Patch-clamp

Patch-clamp is a technique based on voltage-clamp, that allows the study of macroscopic ionic currents in small cells and even single ion channels, using a single recording electrode. In whole-cell configuration, a micropipette is in contact with the cell membrane, which provides electrical and molecular access to the intracellular space. Patch-clamp recordings can be performed on various types of preparations, such as cultured cells or tissue slices. An advantage of the method is that it provides information on how certain, like pharmacological manipulations, may change specific neuronal functions. The experiments can be done either in voltage-clamp mode, in which the voltage is controlled and the resulting currents are recorded, or in current-clamp mode, in which the current is held constant enabling the study of membrane potential. [1, 6]

Ionic conductance is proportional to the ion channel activity, which is an important property of cells. Ion conductance can be studied by measuring the current under voltage-clamp, since the current is linearly proportional to the conductance. Keeping the voltage constant, capacitive current can be eliminated and the time-dependent characteristics of ion conductances can be measured without the influence of voltage-dependence. In voltage-clamp, capacitive current only occurs in the very beginning of the voltage step. Except for this brief charging time, the currents are proportional only to the membrane conductance. [1, 6]

A current-voltage relation (I-V relation) of a cell is obtained with the voltage-clamp method. It is a graph of the measured currents as a function of voltage. It is a useful tool, giving information about conductance, gating properties, ion selectivity and ion concentrations. For example, the reversal potential of an ion channel ($E_i$), can be determined with the I-V relation of the channel. It is the voltage at which the net current is zero; in other words, the point where the graph crosses the x-axis. [1, 6]

### 2.4.1 Patch-clamp set-up

A basic patch-clamp set-up includes a patch-clamp amplifier, a digital-analog and analog-digital converter (A/D converter), a computer as well as recording and reference electrodes. In this section, the components of the set-up are discussed, while the following section focuses on the electrical circuits and adjustments, including electronic compensation, involved in patch-clamp experiments.

Typically, the electrodes used in patch-clamp are made from silver wire coated with silver chloride (Ag/AgCl). The electrons flow from a copper wire to the AgCl wire, converting the AgCl to Ag atoms, while $Cl^-$ ions become hydrated. In Ag/AgCl electrodes, electrons can also flow in the opposite direction, and therefore the Ag/AgCl electrodes are said to be reversible. If electrons flow in the opposite direction, Ag atoms in the wire coated with AgCl give electrons and combine with $Cl^-$ ions, forming insoluble AgCl. The electrode functions as a redox electrode and the reaction occurs between the silver metal and its salt, AgCl. The half reactions can be expressed as

$$Ag^+ + e^- \leftrightarrow Ag(s) \tag{34}$$

and

$$Ag^+ + Cl^- \leftrightarrow AgCl(s) \tag{35}$$

The total reaction is presented as

$$Ag + Cl^- \leftrightarrow AgCl + e^-. \tag{36}$$

Ag/AgCl electrodes are considered having stable potentials at a variety of currents. On the other hand, the reversibility makes them susceptible to exposure of metallic silver, which may lead to junctional effects, electrode instability and motion artifacts. Leaking silver ions could also be poisonous to proteins. Voltage offsets may arise if the reagents in the bath modify the redox reaction of Ag. However, Ag/AgCl electrodes are typically insensitive to the amount and duration of current measured in biological experiments, and when used properly, any significant problems can be avoided. Deterioration of the chloride coating on the electrode wire may also be a source of a slow drift in the signal. Therefore, the silver wire electrodes need to be chlorided regularly. It is also important to use solutions that contain $Cl^-$. Additionally, the patch-clamp amplifiers usually include a pipette offset function, that can be used to correct any voltage error due to the pipette. [8, 9, 10]

The electronic equipment involved in the patch-clamp set-up are a source of noise which should be taken into account, because the recorded signals are typically extremely small, in this case, of the order of picoamperes. First of all, most of the noise can be minimised with a good grounding configuration. In addition, a Faraday cage can be used around the microscope and recording chamber in order to shield the set-up from external interference. A Faraday cage is a mesh of conducting material, which prevents certain types of electromagnetic radiation from entering it. It also works well in making sure that the experimenter avoids any static electricity, before touching any of the electrical components. Furthermore, anti-vibration tables can be used to minimise the effects of mechanical interference. [8]

In a typical voltage-clamp circuit, the reference electrode is placed in the recording chamber that is filled with bath solution that aims to mimic the extracellular solution of the cells. The recording electrode is inserted in a micropipette filled with a solution mimicking the intracellular solution. A perfusion system can also be used, which allows the exchange of the bath solution. It may also be used to apply any pharmacological agents and in general to make sure the cells stay viable, when for example, the metabolic rate of the cells is higher. [8, 9]

The electrodes are connected to a pre-amplifier that is used to measure the membrane potential and inject current. The pre-amplifier is further connected to an operational amplifier. The function of the amplifier is described in more detail in the following section. The signal from the amplifier goes to the computer via an A/D-converter. Therefore, the signals are easy to save and analyse. [6, 8]

The recording electrode is attached to a holder inside a pipette and it can be moved with a micromanipulator. When the recording electrode is immersed into the bath, an offset potential can be observed. The offset potential is a result of the liquid junction potential (LJP), which occurs when two solutions of different ion concentrations are in contact with each other. It can be corrected manually with the pipette offset controls of the amplifier. At this point, an estimate of the electrode resistance ($R_e$) is obtained from the amplifier. [6, 8]

When the recording electrode is in contact with the cell, electrical circuit is formed. There is typically a silicon tube connected to the pipette that allows the control of the pressure inside the pipette. The pressure can be controlled either with a syringe or with mouth. Positive pressure is applied when moving the electrode towards the bath in order to avoid the pipette tip from being contaminated. Negative pressure can be applied to help seal formation. [1, 6, 8]

When the pipette is attached to the cell membrane and a gigaohm seal is obtained, it is referred to as cell-attached configuration. This allows the recording of currents within the patch of the

membrane. An inside-out patch configuration can be obtained when detaching the patch of the membrane that is obtained in cell-attached configuration. This gives access to the intracellular surface of the membrane via the bath solution. [9]

The whole-cell configuration can be achieved with a pulse of suction once a gigaseal is obtained in cell-attached mode. The pulse of suction helps to rupture the cell membrane. In some amplifiers, a zap circuit can also be used. In the zap technique, a large hyperpolarizing voltage pulse, of the order of 1 V, is applied. This generates a dielectric breakdown of the patch of the membrane, providing access to the intracellular part. With some cells, it may be difficult, or otherwise not desirable (e.g., due to mixing of cytosolic content with pipette solution), to go whole-cell. In this case, perforated patch-clamp can be considered instead. Perforated patch-clamp is discussed in more detail later on. [2, 8, 9]

An outside-out configuration can be obtained by pulling the electrode once in whole-cell mode. Therefore, the patch of the membrane is detached from the cell, resulting as an outward patch from the pipette, in which the extracellular side of the membrane faces outward. Schematics of different configurations are shown in Figure 3. [9]

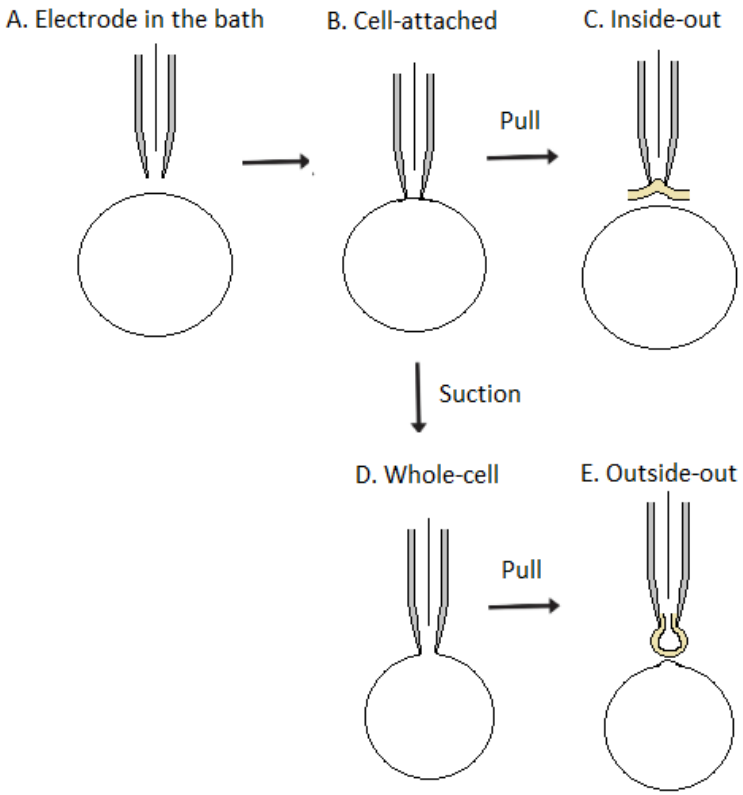


Figure 3: The patch-clamp configurations. *A.* Electrode in the bath. *B.* Cell-attached. *C.* Inside-out. *D.* Whole-cell. *E.* Outside-out.

### 2.4.2 Electric circuits and compensation

In order to control the membrane voltage, an operational amplifier is used as a current-to-voltage converter. It is a differential amplifier, that operates in current follower configuration with negative feedback, in which the inverting input of the amplifier is kept at the command voltage ($V_c$). The electric circuit of the voltage clamp is shown in Figure 4.

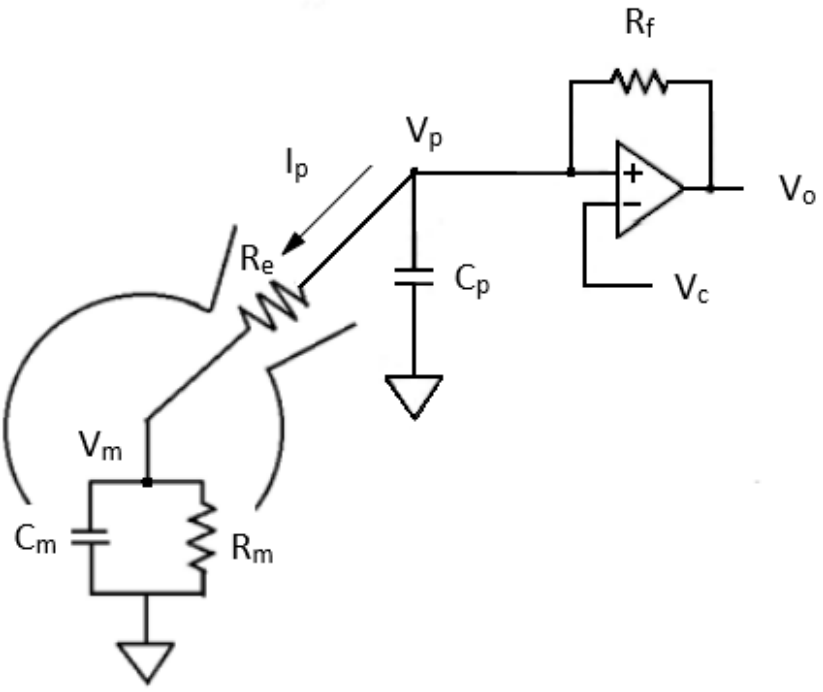


Figure 4: The electric circuit of the voltage-clamp. $C_m$, $V_m$ and $R_m$ are the membrane capacitance, membrane potential and membrane resistance, respectively. $R_e$ is the resistance of the electrode and $I_p$, $V_p$ and $C_p$ are the current, potential and the capacitance of the pipette. $R_f$ is the resistance at the feedback resistor and $V_c$ and $V_o$ are the command and output voltages, respectively.

Any current entering the inverting node must flow via the feedback resistor with a resistance $R_f$. By Ohm's law, the current at the feedback resistor is

$$I_f = \frac{V_o - V_p}{R_f}, \tag{37}$$

where $V_o$ is the output voltage and $V_p$ is the voltage of the pipette. [6, 11]
The output voltage can now be determined as

$$V_o = V_p + I_f R_f. \tag{38}$$

Kirchhoff's current law states that current must be conserved. Therefore, the current at the feedback resistor must be equal to the current flowing out of the pipette, i.e. $I_f = -I_p$. Thus, the output voltage can be given as

$$V_o = V_p - I_p R_f. \tag{39}$$

Since the $V_p$ is kept equal to $V_c$, $V_o$ can be given in terms of the $V_c$ as

$$V_o = V_c - I_p R_f. \tag{40}$$

Furthermore, the current through the pipette can be defined:

$$I_p = \frac{V_c - V_o}{R_f}. \tag{41}$$

Both the cell membrane and the pipette tip act as capacitors. Capacitive current is proportional to the change in voltage, as stated in equation (17). When a voltage step is applied, the current first charges the electrode capacitance ($C_p$). After the $C_p$ is charged, the current can flow through the cell membrane. This is seen as capacitive transients in the signal. These transients may saturate other circuits, which may result in distortion of the signals of interest. The resistance and capacitance of the pipette create a low-pass filtering effect, which shunts high-frequency signals from the pipette to ground. The time constant for the relaxation of the current and voltage is defined as

$$\tau_p = R_p C_p. \tag{42}$$

The transients can be electrically compensated with the $C_p$ compensation, in which current is injected at the input of the amplifier. [6, 8]

The current follower clamps the end of the electrode and therefore any current flowing through the $R_e$ causes a voltage drop. The interaction between the $R_e$ and $C_m$ also creates unwanted filtering effects, which is seen in capacitive transients. This is referred to as series resistance ($R_s$) and it is defined as the sum of $R_e$ and any access resistance ($R_a$) between the pipette tip and the cell. The voltage error ($\Delta V$) between $V_m$ and $V_c$ is dependent on the $R_s$ and $I_m$, which can be expressed as

$$V_m = V_c - R_s I_m. \tag{43}$$

The voltage and current relax to steady state values according to a time constant

$$\tau = R_s C_m. \tag{44}$$

The $R_s$ can be minimized using electrodes with as low a resistance as possible. For homogeneous conducting materials, resistance for a cylindrical block can be determined by

$$R = \frac{\rho l}{A}, \tag{45}$$

where $\rho$ is resistivity ($\Omega m$) that describes the ability of a material to resist electric current, $l$ is the length of the cylinder and $A$ is the cross-sectional area. [3]

The pipettes used in patch-clamp usually have a resistance in the range of 1-10 M$\Omega$. Blunt electrodes are required to achieve stable seals between electrode and the cell membrane. Since the resistance of the pipettes can only be decreased by increasing the size of the pipettes, the

reduction of $R_s$ in this way is limited. Therefore, the electrical $R_s$ compensation is generally used in patch-clamp. [1, 2, 6]

The $R_s$ compensation involves positive feedback and it is used to minimise the effect of $R_s$ and the resulting voltage error. The voltage-clamp is therefore faster, which is important especially when recording fast and inactivating currents, such as $Na^+$ currents. When using the $R_s$ compensation, it should be noted that it adds noise to the $I_m$ signal. Due to the positive feedback, the $R_s$ compensation may cause oscillation, especially if the level of compensation is more than 90%, or the $R_s$ is overcompensated. [6, 8]

Usually, the types of filters used in the amplifiers in electrophysiology are the Bessel filter and the Butterworth filter. The two main considerations when selecting the filter cutoff frequency include aliasing and risetime. Nyquist frequency defines the minimum permissible digitizing frequency by equation

$$f_d \geq 2f_c, \tag{46}$$

where $f_d$ is the digitizing frequency and $f_c$ is the cutoff frequency. In other words, the $f_d$ should be at least twice the filter $f_c$. However, $f_d \geq 5f_c$ is typically used in patch-clamp. In this case, if the filter is at 2 kHz, the sampling rate should be at 10 kHz. [8, 9]

### 2.4.3 Current-clamp

When, instead of measuring the membrane currents, the experimenter wants to record the membrane potential, current-clamp mode can be used. Current-clamp mode detects transmembrane voltage change that results from ion channel activity. This helps to understand the responses of the cells to different stimulation, caused by neurotransmitters, for instance. [6, 8, 9]

The ability of neurons to generate action potentials can be studied with current-clamp. Parameters that are involved in the study of action potentials include the spike threshold, which means the level of excitation that is needed for the cell to produce an action potential. Additionally, neurons have a refractory period, which is a time period after an action potential, during which another action potential can not be generated. [1, 2, 6]

In contrast to voltage-clamp, current-clamp is achieved with a voltage follower. Figure 5 shows the electrical circuit of current-clamp. In I=0 mode of the current-clamp, all external inputs are disconnected. This mode of current-clamp is usually used to check the resting membrane potential of the cell or the electrode offset. Moreover, the PSPs can be studied during neurotransmitter stimulation in the native setting. [8]

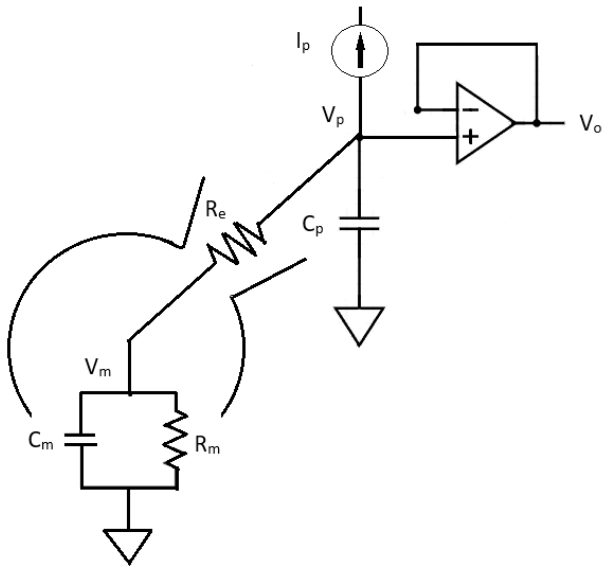


Figure 5: Voltage follower circuit. The operational amplifier is connected to the cell via an electrode with resistance $R_e$ and it contributes to the parasitic capacitance $C_p$. $I_p$ is the injected current. The negative feedback helps to keep $V_o$ equal to $V_p$.

Similarly to voltage-clamp, the electrode resistance creates an unwanted artefact into the recording, since the voltage is recorded with the electrode. Any injected current causes a voltage drop, that is, by Ohm's law

$$V_{err} = I_p R_e. \tag{47}$$

This voltage error, as in the case of voltage-clamp, can be reduced by using larger electrodes with highly-conductive solution. Additionally, since the injected current is known, most amplifiers provide the estimation of $R_s$, which helps to correct the recorded voltage. The voltage error due to the resistance of the electrode can be corrected by bridge balance, in which a current step is injected to adjust the electrode resistance until no instantaneous voltage change occurs at the beginning of the step. Balancing the bridge only modifies the output signal, and hence it does not affect the cell. The effect of the bridge balance is shown in Figure 6. [6, 8]

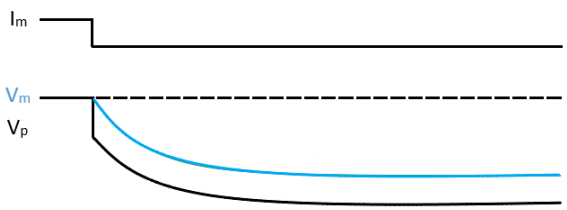


Figure 6: The effect of bridge balance causes the black voltage trace ($V_p$) to shift towards the blue voltage trace ($V_m$), when injecting a current step.

## 2.5 Chloride homeostasis

The intracellular composition of ions in neurons is an important factor in the function of the nervous system. In the CNS, the function of $Cl^-$ channels and transporters is involved in neuronal growth and development, neurotransmitter uptake, intracellular pH modulation and cell volume regulation. The homeostasis of $Cl^-$, the most abundant transportable anion in cells, is a critical factor, especially when it comes to the inhibitory activity mediated by GABAergic and glycinergic transmission. The $Cl^-$ homeostasis is primarily regulated by the cation-chloride cotransporter (CCC) family, as well as $Cl^-$ channels, which are discussed in the following sections. [5, 14, 15, 16]

### 2.5.1 Chloride channels

Ion channels are transmembrane proteins that contain a pore, a specialized structure permitting certain ions to move through the channel down their electrochemical gradient, which is generated and maintained by active ion pumps and exchangers. Ion channels typically provide rapid, highly selective and regulated movement of ions. Voltage-gated ion channels are able to sense the electrical potential across the cell membrane, which regulates the opening and closing of the channels. Opening of a voltage-gated channel results in a flow of specific ions into or out of the cell. In ligand-gated channels, the opening and closing is dependent on the binding of ligands to the receptors on the extracellular part of the membrane. $Cl^-$ channels can be activated in response to changes in either membrane voltage, intracellular pH or intracellular $Ca^{2+}$ signalling. [2, 14, 15, 16]

In general, $Cl^-$ channels are involved in the control of transepithelial transport and membrane excitability. $Cl^-$ channels include the voltage-gated $Cl^-$ channels (ClC), the cystic fibrosis transmembrane conductance regulator (CFTR), and the ligand-gated channels which are activated by neurotransmitters, GABA and glycine. Mutations in $Cl^-$ channels have been linked to disorders such as cystic fibrosis (CFTR), epilepsy (ligand-gated $Cl^-$ channels) as well as inherited kidney stone diseases that are linked to deficiency of ClC channels. Figure 7 shows an overview of the major channels and transporters contributing to $Cl^-$ homeostasis. [14, 16]

GABAergic synaptic inhibition is mediated by two receptor systems, the ionotropic $GABA_A$Rs and metabotropic $GABA_B$Rs. $GABA_A$Rs are ligand-gated channels, that rely on the $Cl^-$ gradients to generate fast inhibitory synaptic currents. $GABA_B$Rs generate slower inhibitory actions via the guanine nucleotide-binding protein (G-protein) coupled receptors (GPCR). [15, 16, 17, 18]

When $[Cl^-]_i$ is low, and $E_{Cl}$ is hyperpolarized in relation to the resting membrane potential of the neuron, GABA opens $Cl^-$ permeable $GABA_A$R channels and hyperpolarizes the neuronal membrane, resulting in inhibitory actions. If $[Cl^-]_i$ is high, and $E_{Cl}$ is more positive than the resting membrane potential, it results in a depolarizing, excitatory action of GABA. Impaired $Cl^-$ channel and transporter function have been linked to multiple genetic disorders, such as epilepsy, which is characterized by hyper-excitability and seizure activity. Thus, $Cl^-$ channels and transporters are important targets as therapeutic tools to balance $[Cl^-]_i$ to help maintain normal neurological activity. Therefore, understanding the mechanisms underlying the regulation of $[Cl^-]_i$ is important in order to decipher the GABAergic and glycinergic signaling in neurons. [14, 15, 16, 17]

The glycine receptors (GlyRs) act as ligand-gated $Cl^-$ channels, mediating excitatory or inhibitory responses, depending on the membrane potential and $E_{Cl}$. GlyRs are present throughout the CNS, especially in the spinal cord, cerebellum, hippocampus, amygdala and hypothalamus,

for example. There are also glycinergic and mixed glycinergic or GABAergic interneurons, which locally innervate principal neurons in the CNS. Most GlyRs are believed to only function during a limited developmental window, contributing to the formation of synaptic connections. An *in vitro* whole-cell patch-clamp study of rats revealed an increase in frequency of excitatory and inhibitory postsynaptic currents upon application of glycine. This implies that ionotropic GlyRs may be expressed in the developing cerebellum and contribute to the organization of cerebellar circuits. [19, 20, 21]

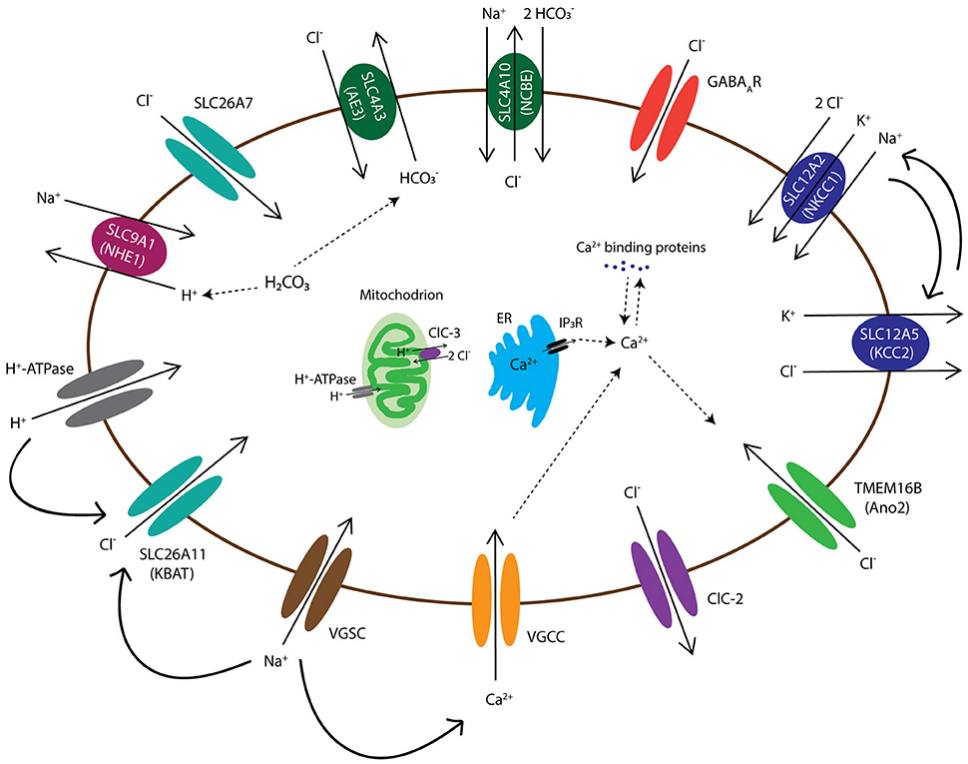


Figure 7: An overview of the channels and transporters contributing to $Cl^-$ homeostasis. Figure adopted from [16].

Acid-base regulation is a homeostatic process crucial for cell survival and tissue function. A significant amount of acid is produced via metabolism, which needs to be buffered. The transporters regulating pH include $Cl^-$/bicarbonate ($HCO_3^-$) exchangers, such as SLC26A7 channel, and $Na^+/H^+$ exchangers, for example. [16]

Some cells expressing $Cl^-/HCO_3^-$ exchangers are highly acidic and need another pathway for $Cl^-$ recycling, whereas other cells such as intestinal cells use the polarized expression of $Cl^-$ channels and secondary active $Cl^-$ uptake mechanisms to transport water and salts across the apical membrane. This transport is maintained by $Na^+$-$K^+$-$2Cl^-$-cotransporters which maintain high $[Cl^-]_i$. [14, 16]

Members of the ClC family are involved in a variety of cellular functions. ClC-1 is encoded by the *CLCN-1* gene and it is known for its high $Cl^-$ conductance. It is primarily expressed in skeletal muscles, maintaining the resting potential of the sarcoplasmic reticulum and repolarization after contraction. Additionally, recent studies have identified mRNA and protein expression of the channel in neuronal tissue, including pyramidal cells of the hippocampus and brain stem nuclei. [14, 16]

ClC-2 is activated by swelling, acidic pH and hyperpolarization. The functioning of ClC-2 regulates $[Cl^-]_i$, cell volume and neuronal excitability. ClC-2 is broadly expressed in the body. In the brain, it has been found in a variety of neurons, such as pyramidal cells of the hippocampus and glial cells in the cerebellar cortex. [14, 16]

Members ClC-3 to ClC-7 are predominantly distributed in intracellular organelles. The ClC channels found in the plasma membrane have been linked to participate in stabilizing the membrane potential and $[Cl^-]$ across the membrane. In contrast, ClC channels in the intracellular organelles act as electrogenic $Cl^-/H^+$ exchangers facilitating endosomal and vesicular acidification. [14, 16]

### 2.5.2 Cation-chloride cotransporters

Ion cotransporters are secondary active transporters, which indirectly use the energy from the hydrolysis of ATP to carry two different ions or molecules across the membrane, using the electrochemical gradient of one solute to transport the other ion or molecule against its gradient. The members of the CCC family, encoded by the *Slc12a1-9* genes, include seven plasmalemmal ion transporters, which are the $Na^+$-$K^+$-$2Cl^-$ cotransporters type 1 and 2 (NKCC1 and NKCC2), $Na^+$-$Cl^-$ cotransporter (NCC) and $K^+$-$Cl^-$ cotransporter types 1-4 (KCC1-4). All CCCs, except for NKCC2 and NCC, are found in the brain. They are also expressed in specific cell types, brain regions and developmental stages. NKCC1 and KCC2 are the major regulators of $Cl^-$ homeostasis. The developmental shift in the function of the two transporters and their contribution to $Cl^-$ homeostasis is shown in Figure 8. [5, 15, 16, 17, 19]

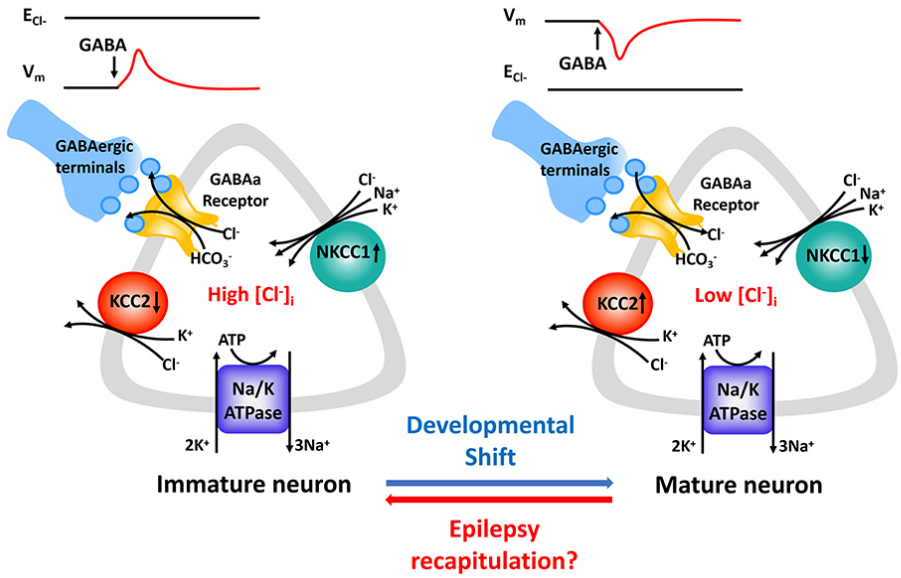


Figure 8: The developmental shift in GABAergic function due to the change in expression levels of NKCC1 and KCC2. In a developing neuron (on the left), the activity of KCC2 is relatively low as opposed to the activity of NKCC1, resulting in a higher $[Cl^-]_i$. On the right, is a schematic of a mature neuron, in which the activity of KCC2 is increased, while the activity of NKCC1 is decreased. This results in a lower $[Cl^-]_i$ and a hyperpolarizing, inhibitory action of ligand-gated $GABA_A$ receptor. Figure adopted from [19].

NKCC1, encoded by *Slc12a2*, symports $Cl^-$ into cells in a 1:1:2 stoichiometry, and is therefore an electroneutral carrier. NKCC1 is the dominant $Cl^-$ transporter during early development, maintaining a high $[Cl^-]_i$. [5, 15, 17, 18, 19]

In contrast to NKCC1, KCC2, encoded by *Slc12a5*, uses the gradient of $K^+$ to extrude $Cl^-$ in a 1:1 stoichiometry, maintaining the driving force for the $Cl^-$ permeable $GABA_AR$. KCC2 is the only CCC that is primarily expressed in neurons and its expression is also characterized by progressive increase during development. Upon activation of the $GABA_AR$, $Cl^-$ flows into the neuron hyperpolarizing the membrane. This action is required for fast synaptic inhibition in the mature CNS. Moreover, KCC2 has a structural role in cell migration, dendritic outgrowth, spine morphology and formation of synaptic connections. There are two splice variant proteins of KCC2, KCC2a and KCC2b, which is a result of alternative splicing. The two isoforms only differ in their first exons. KCC2b participates in generating the hyperpolarizing $GABA_AR$-mediated transport. [4, 15, 17, 19, 20, 21, 22]

Both NKCC1 and KCC2 are formed by 12 transmembrane segments, 6 extracellular loops and intracellular N- and C-terminals. However, the position of regulatory sequences, phosphorylation sites and extracellular loops are different between them.

Since pathophysiological activities associated with various neurodevelopmental disorders have been linked to the deficiency of KCC2-mediated $Cl^-$ homeostasis, it makes it an important target of study. Previous studies have shown the protein kinase C (PKC) to be in a central role when it comes to the phosphorylation of KCC2. Phosphorylation is a post-translational modification, during which a phosphate group attaches to a molecule, altering the structural conformation of a protein. Phosphorylation can lead to either activation or deactivation of a protein. In the case of KCC2, its activity is strongly inhibited by phosphorylation of two C-terminal residues, $Thr^{906}$ and $Thr^{1007}$. [5, 15, 19, 20, 22]

## 2.6 Approaches to study $Cl^-$ homeostasis

A variety of proteomic, biochemical, molecular and electrophysiological methods can be used to study the mechanisms underlying the regulation of $Cl^-$ homeostasis. These include flame photometry, that was one of the first methods used to measure changes in the $[K^+]_i$, $[Na^+]_i$ and $[Cl^-]_i$. Quinolinium halid-sensitive fluorescent indicators are sensitive and selective for $Cl^-$ and they can be used to visualize changes in $[Cl^-]_i$. Some limitations in the quinolinium dyes arise due to their strong bleaching rate and leaking from the cells. Quinolinium halid-sensitive fluorescent indicators have not been used to systematically analyse the activity of NKCC1 or KCC2. [5]

Other $Cl^-$-sensitive indicators include the family of derivatives of yellow fluorescent protein (YFP), which show halid-dependent changes in their fluorescence intensity. $NH_4^+$ flux assay, on the other hand, relies on the measurement of $NH_4^+$-dependent changes of the intracellular pH. Other $K^+$ surrogate methods are based on the use of thallium ($Tl^+$) or the radioactive rubidium ($^{86}Rb^+$). The advantages of $K^+$ surrogate methods include a precise estimation of the activity of NKCC1 during short periods of time, in seconds, and under conditions that are close to physiological ones. [4, 17]

Perforated patch-clamp is a technique that is based on the use of a pore-forming agent, such as antibiotic gramicidin. In gramicidin perforated patch-clamp (GPPC), gramicidin is added to the pipette solution and when in contact with a cell, it forms cation-selective pores in the membrane. Therefore, electrical contact can be achieved with the cytoplasm without affecting the $[Cl^-]_i$ or other intracellular metabolites. Activation of $GABA_A$ or glycine currents on the postsynaptic membrane produce ion fluxes that are dependent on the ratio between the $[Cl^-]_i$ and $[Cl^-]_o$ as well as the $V_m$. An I-V relation is therefore obtained, and the reversal potential of $Cl^-$-permeable $GABA_A$ or glycine receptor channels can be determined. The $[Cl^-]_i$ can be calculated using the Nernst equation (10),

$$[Cl^-]_i = [Cl^-]_o e^{\frac{E_r}{(RT/zF)}},$$

since the $[Cl^-]_o$ is known. [5, 8]

An advantage of GPPC is that it allows a good estimation of $[Cl^-]_i$ at the single cell level. However, some limitations arise, which must be taken into account. Firstly, the method affects the $[K^+]_i$, which is the main co-carrier of $Cl^-$. Another factor affecting the results is the $V_H$ of the voltage-clamp, that contributes to the driving force of $Cl^-$. [4, 5, 17]

Another, non-invasive approach is the cell-attached configuration of patch-clamp. It allows to determine a single $GABA_AR$ channel currents. The reversal potential of a single $GABA_AR$ helps to determine the difference between $E_{GABA}$ and $E_m$, or the driving force of $GABA_A$. Thus, $[Cl^-]_i$ can be calculated as described for the GPPC. [4, 5]

Studies done with GPPC have shown that the downregulation of KCC2 leads to a depolarizing shift in the $GABA_AR$ responses. For example, in the study by Goutierre et al. [22], the values of $E_{GABA}$ were -82.0 $\pm$ 2.2 mV and -74.2 $\pm$ 2.7 mV for cells expressing KCC2 and KCC2 knockdown neurons, respectively. In addition, the KCC2 knockdown neurons displayed more depolarized $V_{rest}$ of -83.6 $\pm$ 1.5 mV, compared to the control value of -89.8 $\pm$ 0.8 mV. In another study by Acton et al. [23], $E_{Cl}$ was determined at -97.56$\pm$4.49 mV with cells expressing KCC2, whereas in the untransfected control cells it was -58.44$\pm$2.95 mV.

In the next section, the use of different cell lines as the expression systems is discussed more.

## 2.7 Cell lines as expression systems

When studying the expression of exogenous ion channels with the patch-clamp method, it is important to know what type of cells should be used, since the cells are used as the biological environment to provide the machinery for protein synthesis. Usually, the studies of ion channel function are done using the expression of cloned channels in mammalian cells. [24, 25, 26, 27, 28]

Transfection is a technique that is used to insert foreign nucleic acids into cells that are used as the expression system. Transfection is based on the use of either a viral or non-viral vector, such as plasmid, to transport the desired DNA into the host cell. RNA can also be transported into eukaryotic cells via RNA-based viral or non-viral vectors. The transfection of RNA is more likely to result in higher transfection efficiency as the DNA transfection, since RNA does not need transport across the nuclear membrane. The process of RNA transfection is also faster compared to DNA transfection, because there is no need for the genome integration, transcription nor the post-transcriptional processing. However, RNAs are less stable than DNAs, making them more prone to degradation during transfection. [25, 26, 27]

Transfection methods include chemical, biological and physical transfection. Chemical transfection is based on the use of cationic reagents to deliver the wanted DNA into cells. In contrast, biological transfection methods rely on the use of viral vectors, whereas physical transfection methods rely on microinjection, electroporation or ultrasound, for example. [25, 26, 27]

The functional properties of membrane currents can be distinguished by their ion selectivity, current-voltage relationships and activation or inactivation properties, for example. The functional diversity of ion conductances at the whole-cell level has shown to be important in the classification of ion channels. [25, 26, 27]

With the patch-clamp method, there are several cell lines that have been used as expression systems, such as Xenopus oocytes, Chinese hamster ovary (CHO) cells, human embryonic kidney (HEK293) cells and various neuroblastoma cell lines. An advantage in using mammalian cells is that the transcription, translation and post-translational mechanisms are conserved. For example, HEK293 cells are suitable for the study of ion channels that are only expressed in excitable cells. Their relatively small cell size, morphology and division rate are highly suitable for patch-clamp and gigaseals can be formed easily. HEK293 cells have relatively low expression of native channels and they also have a high transfection efficiency. [28, 29]

The human SH-SY5Y neuroblastoma cell line is used as a neuronal cell model. After differentiation to a neuron-like state, SH-SY5Y cells are morphologically similar to neurons, forming functional synapses. SH-SY5Y cells have shown to be able to differentiate towards cholinergic, dopaminergic and adrenergic fate. Advantages in using SH-SY5Y cells are that they are an immortalized cell line, so they can continue proliferating and they are also relatively simple to modify genetically and so they provide a system for the study of diseases. Moreover, because they are human-origin, the SH-SY5Y cells express human-specific proteins. In study by Meyer and Heinemann [30], the voltage threshold for activation of the human Erg $K^+$ channel in the SH-SY5Y cells was studied, and it reportedly changed during different phases of the cell cycle. The results indicated that this would potentially affect the variation of the resting membrane potential of the cells. [30, 31]

The ND7/23 is a hybrid cell line, derived from mouse neuroblastoma cells and rat neuron cells. They have been used to express neuronal ion channels, such as Nav channels, that are resistant to heterologous expression in CHO cells or HEK293 cells. The advantage in using the ND7/23 cells

is that they provide endogenous factors and signalling pathways to promote ion channel peptide folding, expression and cell surface function. They also express native TTX-sensitive voltage-gated $Na^+$ (Nav) currents, and Nav1.2, Nav1.3, Nav1.6 and Nav1.7 transcripts have been shown to be present by molecular profiling. [32, 33]

### 2.7.1 N2a cells

The N2a cell line, which is used for the experiments in this thesis, is a mouse neural crest-derived cell line. In general, N2a cells have been used to study neuronal differentiation, neurite growth and signalling pathways, for example. An advantage in N2a cells is their ability to quickly, within hours, respond to serum removal and other factors in their environment by expressing signalling molecules which results in neuronal differentiation and growing of neurites. N2a cells are known to express some Nav channels, as well as voltage-gated $K^+$ (Kv) channels, which are discussed in more detail in the following sections. [34, 35, 36]

N2a cells mainly express Nav1.2, Nav1.3, Nav1.4 and Nav1.7 channels. Additionally, Erg-mediated $K^+$ channels are also present in N2a cells. With the use of TEA blocking the Kv channels, a study by Wu et al. [34] measured the sodium current with peak amplitude of approximately 830 pA. The values for $G_{Na_{max}}$, $V_{1/2}$ and $k$ were 36.1 $\pm$ 1.2 nS, -24.1 $\pm$ 1.1 mV and 14.0 $\pm$ 0.9, respectively. The resting membrane potential of neuroblastoma cell lines, including the N2a cell line, is typically between -48 to -20 mV, based on previous studies. [35, 36, 37]

Iwata et al. [36], showed that a transient inward current was mediated by $Na^+$, which was blocked by 1 $\mu$M TTX. A sustained outward current was characterized by slow activation and little to no inactivation over 100-200 ms. It was blocked by 20 mM TEA, indicating that the current was mediated by the delayed rectifier $K^+$ channel, which activated at -10 mV. The study found no evidence of activation of $Ca^{2+}$ channels, which was studied using 5 $\mu$M nifedipine, 100 $\mu$M $Ni^{2+}$ and 100 $\mu M$ $Cd^{2+}$, which act as $Ca^{2+}$ channel blockers. For $Na^+$, current with peak amplitude of 1071 pA was recorded. The reversal potential of $Na^+$ was measured at 64.8 mV and the half-maximum activation potential was -23.1 $\pm$ 0.9 mV. The values of $G_{Na_{max}}$ and $k$ in control cells were 14.0 $\pm$ 0.9 nS and 2.0$\pm$ 0.2, respectively. The mean input resistance was 2.23 $\pm$ 0.26 G$\Omega$ and the mean $C_m$ was 31.8$\pm$ 1.8 pF. [36]

### 2.7.2 Voltage-gated potassium channels

The family of $K^+$ channels is a large and the most diverse class of membrane proteins. The family of voltage-gated Kv channels is the most diverse group of these, including 12 subfamilies (Kv1-Kv12). Neurons express different types of Kv channels, that are transmembrane channels transporting $K^+$ across the membrane and sensitive to changes in membrane potential. The equilibrium potential of Kv channels is usually below the resting membrane potential of a neuron and therefore the opening of Kv channels typically repolarises the membrane after an action potential. The function of Kv channels is involved in a variety of cellular processes, such as the functioning of excitable cells, regulation of apoptosis as well as cell growth and differentiation. Deficiency of the functioning of Kv channels is linked to some severe genetic disorders, and thus the understanding of the mechanisms of Kv channel functioning is important. [1, 38, 39]

Each Kv channel gene encodes one $\alpha$-subunit (Kv$\alpha$). To form a functional channel, four $\alpha$-subunits are needed. The structure of an $\alpha$-subunit is shown in Figure 9. The transmembrane domain of the $\alpha$-subunit includes six helices that form two functionally different parts of the channel, a $K^+$ ion-conducting pore-domain (PD) and a voltage-sensing domain (VSD) that is

sensitive to changes in the membrane potential. The PD includes a channel gate and a selectivity filter, which only allow $K^+$ ions to move through the channel. The VSD is formed by the S1-S4 segments, whereas the PD is formed by the P-loop and the S5-S6 segments. The N- and C-termini form the cytoplasmic part of the Kv channels, which do not contain highly conserved regions. The cytoplasmic region is different in Kv channels, compared to other $K^+$ channels. [38, 39]

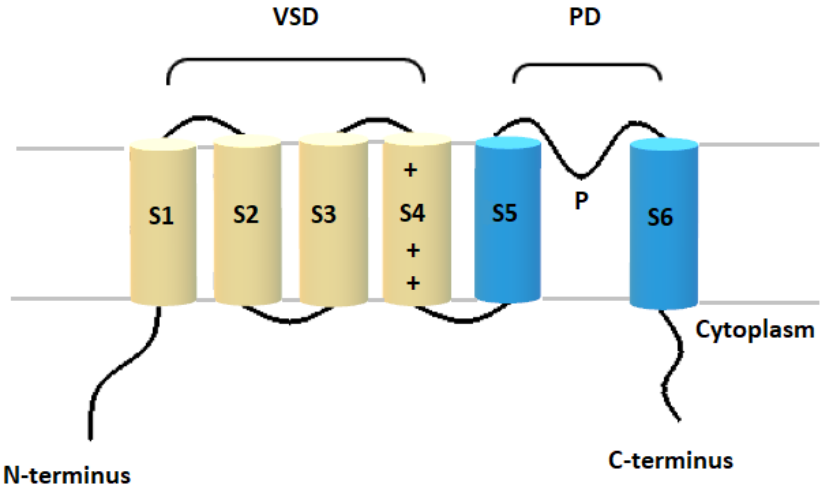


Figure 9: The structure of an $\alpha$-subunit of a Kv channel. VSD is the voltage-sensing domain, including helices S1-S4, and PD is the pore domain, consisting of helices S5-S6 and the P-loop.

Mutations in the genes of Kv channels can cause severe disorders, including epilepsy and cardiac rhythm disorders. Therefore, the understanding of the structure and function of Kv channels is important. In addition, they act as perspective drug targets, so the understanding of the functioning helps the search of new drugs. [38, 39]

Kv channels have three functional states: closed, open and inactivated state. The channels are usually closed in the resting state, in which they do not conduct ions. As the membrane is depolarized, its intracellular part is positively charged, which results in conformational rearrangements of Kv channels, making the open conformation more favourable and the channel activates. If the membrane remains depolarized, most of the channels inactivate. [38, 39]

In Kv channels, two inactivation types can be distinguished, the N-type inactivation and C-type inactivation. Fast N-type inactivation is mediated by an inactivation peptide that is folded and attached by a linker to the N-terminus of an $\alpha$-subunit or a $\beta$-subunit. The inactivation peptide enters the open pore and blocks any ion transport. The slow C-type inactivation occurs when the selectivity filter acts as the second gate and closes, blocking ion traffic. The channels switch from inactivated state to the closed conformation when the membrane potential drops to the level of the resting membrane potential. [38, 39]

Kv2.1 constitutes the predominant delayed rectifier $K^+$ channels in many cell types. Kv2.1 has shown to be present in almost all neurons in the brain. Thus, it maintains the membrane potential as well as neuronal excitability. The activation of Kv2.1 has a high threshold and it is characterized by slow activation and inactivation kinetics. It is also sensitive to TEA. [38, 39]

The *ether-á-go-go* (*eag* or *KCNH*) family of Kv channels (KCNH) includes three gene subfamilies: *eag* encoding Kv10 with two mammalian members (Kv10.1 and Kv10.2), *eag*-related gene (*erg*; Kv11.1, Kv11.2 and Kv11.3) and *eag*-like gene (*elk*; Kv12.1, Kv12.2 and Kv12.3). In mammals, Eag channels are neuron-specific and expressed in the brain, while Erg channels are also expressed in the heart. Opening of Eag channels drives the membrane potential towards the equilibrium value for $K^+$ as for all Kv channels, hence repolarizing action potentials and setting the resting membrane potential. They also switch between the open and closed conformations based on changes of the membrane potential, sensed by the VSD. [40, 41, 42]

In Eag channels, the long cytoplasmic N- and C-terminal ends include specific structural domains that are not found in other Kv channels. These are a Per-Arnt-Sim (PAS) domain with a PAS-cap region in the N-terminal region and C-terminal C-linker domain as well as a cyclic nucleotide-binding homology domain (CNBHD) in the C-terminal region. The PAS domain together with the cap sequence are called the Eag domain. The interaction of the two domains is involved in some of the characteristic gating properties of Eag channels. The structure of an Eag channel is shown in Figure 10. [40, 41, 43]

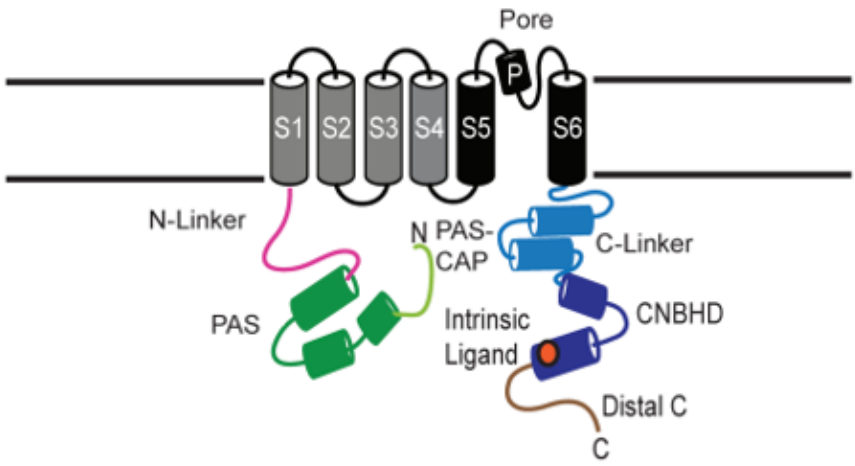


Figure 10: The structure of a subunit of a KCNH channel. VSD is the voltage-sensing domain, including helices S1-S4, and PD is the pore domain, consisting of helices S5-S6. Figure adopted from [41].

Eag channels are characterized by delayed rectifier currents in heterologous expression systems. For Eag channels, slowed activation with a hyperpolarized holding potential is a characteristic feature. Mammalian Eag channels show little or no voltage-dependent inactivation. [40, 41, 42]

Erg channels have unique kinetics compared to other Kv channels. Their inactivation rates exceed activation rates and the maximum conductance is achieved with repolarization, instead of depolarization. [41, 42, 43, 44, 45]

Erg1, encoded by *KCNH2*, in contrast to other KCNH channels, is expressed in the mammalian myocardium, contributing to the native delayed rectifier current. Erg1 channels have slow activation, rapid inactivation and recovery from inactivation. The slow deactivation gives rise to the characteristic inward tail current with repolarization, and it is therefore an inward recti-

fier, only mediating little outward current during depolarization. Two subunits, Erg1a and Erg1b, can be distinguished from Erg1. Mutations in either Erg1a or Erg1b result in Type 2 Long QT syndrome (LQTS2), which is characterized by prolongation of the QT interval in the heart. The voltage-dependence of activation of the Erg channels can be determined by using depolarising pulses applied from a holding potential, and then measuring the resulting tail currents at a hyperpolarizing voltage. [45, 46, 47]

Erg2 and Erg3 are widely distributed in the central nervous system. Erg currents contribute in spike frequency in neurons. The currents of Erg2 are similar to the currents of Erg1, whereas Erg3 has a hyperpolarization-shifted voltage-activation relationship. [45, 46, 48]

### 2.7.3 Voltage-gated sodium channels

The family of voltage-gated sodium channels (Nav) includes members Nav1.1-1.9 encoded by the *SCN1A-SCN5A* and *SCN8A-SCN11A* genes. Nav channels mediate the initiation and propagation of action potentials in excitable cells. Mutations in Nav channels have been linked to some neurological diseases, such as epilepsy (Nav1.1, Nav1.2) and multiple sclerosis (Nav1.6). Therefore, Nav channels are important molecular targets of drugs used in local anesthesia and in the treatment of Nav channelopathies in the brain and heart. The Nav channel subtypes can be classified based on the structure, electrophysiological function, coding gene and TTX-resistance. TTX-sensitive channels include Nav1.1-Nav1.4, Nav1.6 and Nav1.7. [49, 50, 51]

A glycosylated, large pore-forming $\alpha$-subunit with 1-4 smaller $\beta$-subunits are needed to form a Nav channel. The $\alpha$-subunit consists of four homologous, transmembrane domains (DI-DIV), which include six transmembrane segments (S1-S6), three intracellular loops and the N-terminus and C-terminus. The segment S4 acts as the voltage sensor and it is supposed to be related to the activation of a Nav channel. However, the main regulators of the channel function are the N- and C-termini. Figure 11 shows the structure of a Nav channel. [50, 51]

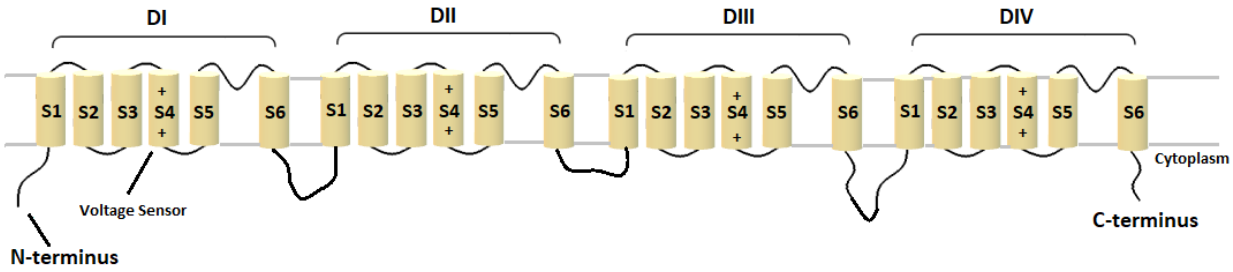


Figure 11: The $\alpha$-subunit of a Nav channel including the homologous transmembrane domains DI-DIV.

The distinct states of Nav channels include the resting closed state, activated open state and the inactivated closed state. In each domain, the S4 segments are able to sense changes in membrane potential. Above a critical threshold, the S4 segments move towards the extracellular surface of the cell membrane, triggering a series of conformational changes which results in channel activation.

The current passing through the channel pore creates the depolarising phase of the action potential. Both the activation and inactivation of Nav channels is generally fast; the activation within 1 ms and inactivation within 1-2 ms. Therefore, the fast activating and inactivating sodium channels are one of the main type of ion channels present in axons besides the delayed rectifier channels. [50, 51]

Nav1.7, that is also expressed in N2a cells and is encoded by *SCN9A* gene, is expressed in the neurons of the peripheral nervous system. It has also shown to be present in pain-sensing, nociceptive neurons at dorsal root ganglion (DRG). Nav1.7 can be characterized by a rapidly activating and inactivating current, which is sensitive to TTX. Mutations in Nav1.7 have been linked to inherited erythromelalgia, that is a rare autosomal dominant inflammatory disease, that includes intense pain. Nav1.7 has shown to exhibit a slow development of closed-state inactivation, which allows the channel to respond to small and slow depolarisations. It is therefore thought to act as a threshold channel that sets the gain in nociceptors. [52, 53]

# 3 Materials and methods

## 3.1 N2a cells

The following experiments were done using cultured commercial neuroblastoma (N2a) cell line. The cells were stored in liquid nitrogen, from which they were thawed in water bath. The cells were moved to a falcon tube filled with cell culture medium (EMEM, DMEM, 10 % fetal bowine serum (FBS), 1% penicillin-streptomycin (PS), 1% Glutamax) with a Pasteur pipette. The cells were centrifuged for five minutes, after which the supernatant was carefully removed, leaving the pellet of cells at the bottom of the tube. Cell culture medium was added into the falcon tube and the cells were suspended properly. The suspension was put in an incubator in a Petri dish.

After a couple of days, the medium was removed and the cells were washed with phosphate buffered saline (PBS). Trypsin was added to detach the cells from the Petri dish. The cells were kept in the incubator for about ten minutes. The growth medium was then added to inactivate the trypsin, after which the cells were suspended. The suspension was added to 35 mm dishes, with coverslips, filled with cell culture medium. The ratio of the suspension and the medium was determined based on the amount of cells. The passage of the cells used in the recordings was between 4-6. One of the recorded cells is shown in Figure 12.

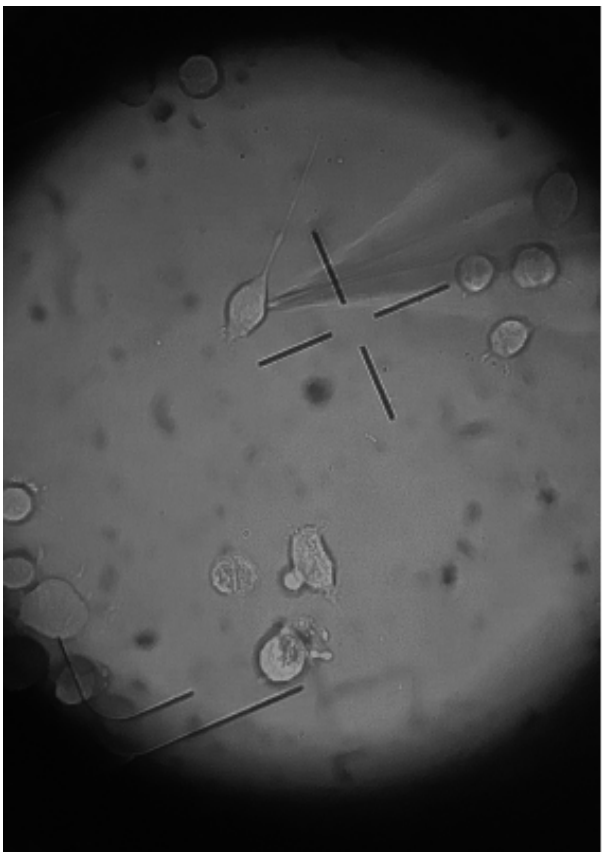

Figure 12: One of the recorded cells in contact with the pipette.

## 3.2 Electrophysiology

The whole-cell patch-clamp recordings of the cultured N2a cells were performed with Model 2400 Patch Clamp Amplifier (A-M Systems, Inc.). The micropipettes were pulled from borosilicate glass capillaries with Model P-87 Flaming/Brown micropipette puller (Sutter Instrument Co.). The Ag/AgCl electrodes were inserted into micropipettes with resistances between 4-6 MΩ. The data were filtered at 2 kHz and sampled at 10 kHz. $R_s$ compensation was adjusted to 80%, unless stated otherwise. A picture of the set-up is shown in Figure 13.

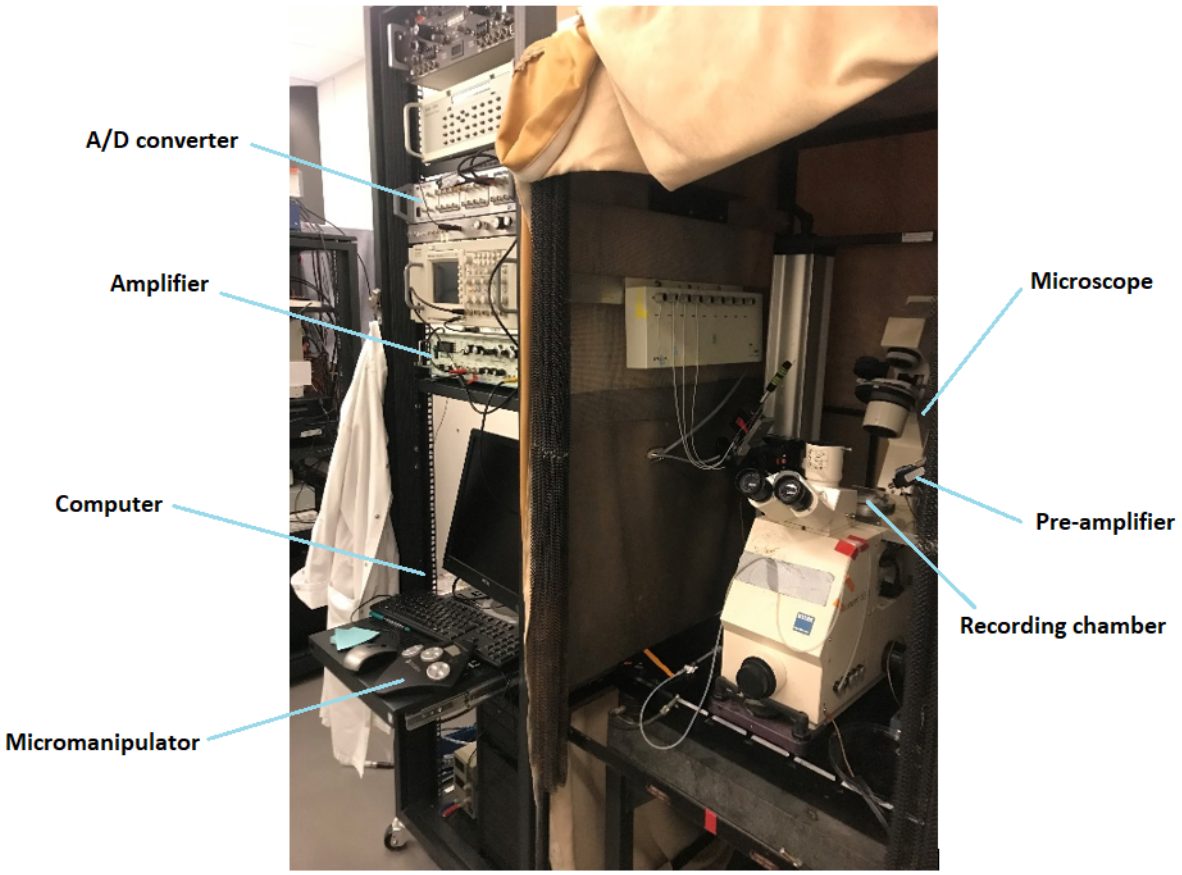


Figure 13: The set-up used in the experiments.

The cells were transferred to the recording chamber filled with bath solution containing the following (in mM): 135 NaCl, 5 KCl, 10 HEPES, 10 glucose, 2 $CaCl_2$, 1 $MgCl_2$. The pH of the bath solution was adjusted to 7.4 with NaOH. The osmolality of the solution was 288 mOsm/kg, measured with Model 3320 Osmometer (Advanced Instruments, Inc.).

The pipettes were filled with pipette solution containing the following (in mM): 140 KCl, 10 HEPES, 3 Mg-ATP. The pH of the pipette solution was adjusted to 7.4 with KOH. The osmolality of the solution was 274 mOsm/kg. The theoretical liquid junction potential of the solutions was 4.6 mV, calculated with Junction Potential tool from pClamp and it is taken into account in the analysis and the results.

For the experiments of Erg currents, the bath solution contained the following (in mM): 100 NaCl, 42.5 KCl, 10 HEPES, 2 $MgCl_2$, 2 $CaCl_2$. pH was adjusted to 7.4 with NaOH.

The pipette solution was the same as described above.

Once a suitable cell was found, and the electrode was in the bath, $R_e$ was checked with a 1 mV test pulse series using the membrane test tool of Clampex of the pClamp software. If needed, the pipette offset was corrected from the amplifier. When in contact with the cell, negative pressure was applied to the pipette to help seal formation. As a stable seal was formed, $R_{seal}$ was checked and more negative pressure was applied in order to rupture the cell membrane. As the whole-cell configuration was achieved, $V_{rest}$ was measured with the I=0 mode for one minute, from which the mean values are used in the analysis and results. After this, $C_m$ and $R_s$ were compensated. Then, five different voltage protocols (I-V; see figures 14-18) were used to study the currents in the cells. The values of $C_m$ and $R_s$ were checked from the amplifier before recordings.

The data analysis is done using Clampfit (Molecular Devices), Excel (Microsoft) and OriginLab 2022. The results are presented as mean $\pm$ standard deviation. The error bars in I-V relations and conductance-voltage graphs indicate the standard deviation. In box charts, the black dots represent the data points, the rectangular dot represents the mean, the line represents the median, the whiskers represent the minimum and maximum values and the box is determined by the 25th and 75th percentiles.

Protocol 1, shown in Figure 14, was used to record the delayed rectifier currents. The holding potential was set to -70 mV to make sure it is within a passive range of the membrane potential. A depolarizing pulse of 0 mV was used in order to inactivate the fast activating Nav and Kv channels, which was followed by test pulses from -80 mV to +55 mV or +85 mV with 15 mV increments.

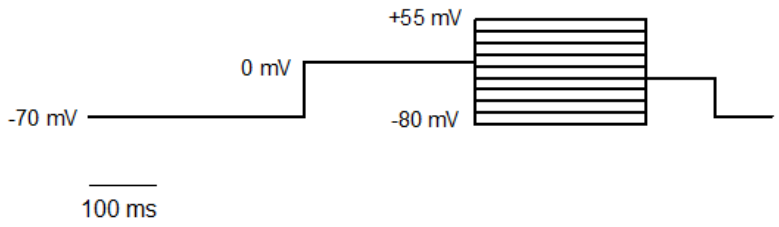


Figure 14: Voltage protocol 1.

For I-V relations, recorded steady state currents at each $V_m$ were normalized against membrane capacitance and are expressed as pA/pF.
Conductances for the steady state $K^+$ currents were calculated at each voltage by the equation

$$g_K = \frac{I_K}{(V_m - E_K)}, \tag{48}$$

where $I_K$ is the mean current at steady state, $V_m = V_c - V_{ljp}$ is the clamped potential and $E_K$ is the reversal potential of $K^+$, which can be calculated from the Nernst equation (10)

$$E_K = \frac{RT}{zF} ln \frac{[K]_{out}}{[K]_{in}} = \frac{8.314J/(K \cdot mol) \cdot (273.15+22)K}{96485.332As/mol} ln\left(\frac{0.005M}{0.140M}\right) = -84.7mV$$

Figure 15 shows the voltage protocol 2, which was used to remove the inactivation of the fast activating Nav channels. The holding potential was set to -70 mV. The removal of inactivation was done using a hyperpolarizing voltage pulse of -100 mV, which was followed by varying voltage steps from -80 mV up to either +55 mV or +85 mV, with 15 mV increments.

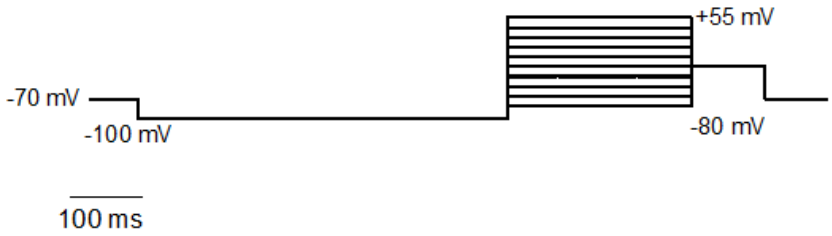


Figure 15: Voltage protocol 2.

During the analysis, currents recorded with protocol 1 were subtracted from the currents recorded with protocol 2, so that only the fast activating and inactivating currents were left. The currents in the I-V relations are the peak Nav currents at each $V_m$, which were normalized against $C_m$ and are thus expressed as pA/pF.
The conductances of Nav channels were calculated from the recorded peak currents at each voltage by the equation

$$g_{Na} = \frac{I_{Na}}{(V_m - E_{Na})}, \tag{49}$$

where $E_{Na}$ was approximated by extrapolating the I-V relation, since there was no $Na^+$ added to the pipette solution. Conductances were normalized to $g_{max}$ and plotted against $V_m$.
Conductance-voltage curves were fitted with Boltzmann equation

$$y = A2 + \frac{A1 - A2}{1 + e^{(V_m - V)/k}}, \tag{50}$$

where $k = -\frac{zF}{RT}$ represents the slope factor. The half-activation potential ($V_{1/2}$) and the slope factor $k$ were determined from the Boltzmann equation.

The expression of Eag- and Erg-mediated $K^+$ currents was also studied. Voltage protocol 3 was used to study the expression of Eag currents. The $V_H$ was set to -70 mV. Varying test pulses were from -120 mV to -40 mV with 20 mV increments, which were followed by a depolarizing voltage pulse of +50 mV, as shown in Figure 16.

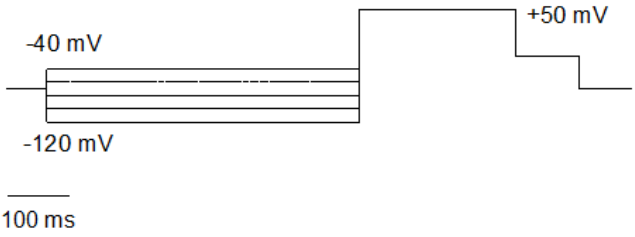


Figure 16: Voltage protocol 3.

Figure 17 shows the voltage protocol 4 for the experiments of Erg tail currents, in which $V_H$ was set to -60 mV. Varying test pulses were from -70 mV to 0 mV with 10 mV increments, which were followed by a hyperpolarizing pulse of -120 mV.

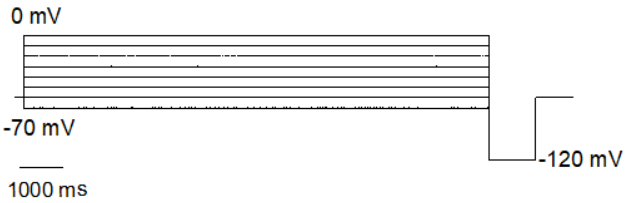


Figure 17: Voltage protocol 4.

The native currents of the N2a cells were studied with voltage protocol 5, with varying $V_c$ from -100 mV to 0 mV with 10 mV increments, as shown in Figure 18. $V_H$ was set to -60 mV, which is typical in the experiments measuring $E_{Cl}$. Each cell ($n$=7) was recorded with and without compensation.

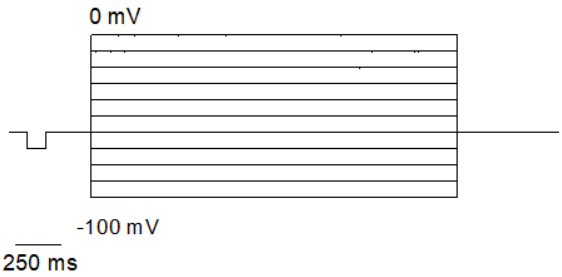


Figure 18: Voltage protocol 5.

# 4 Results

## 4.1 Kv currents

The experiments revealed a few types of Kv currents, presumably mediated by Kv2.1, Eag and Erg channels. These results could be expected based on previous studies. N2a cells are also known to express fast activating A-type Kv currents, but they were not studied specifically, since they are likely to overlap with the fast activating Nav currents. Therefore, Nav channel blockers such as TTX, could be used to study them.

### Delayed rectifier

The analysis of the delayed rectifier currents is done separately for two groups, based on the used $V_c$. For Group 1, the $V_c$ was set from -80 mV up to +55 mV and for Group 2 from -80 mV up to +85 mV. Figure 19 shows the delayed rectifier current traces recorded from Cell 1 as an example from Group 1. I-V relation of the cell is shown in Figure 20.

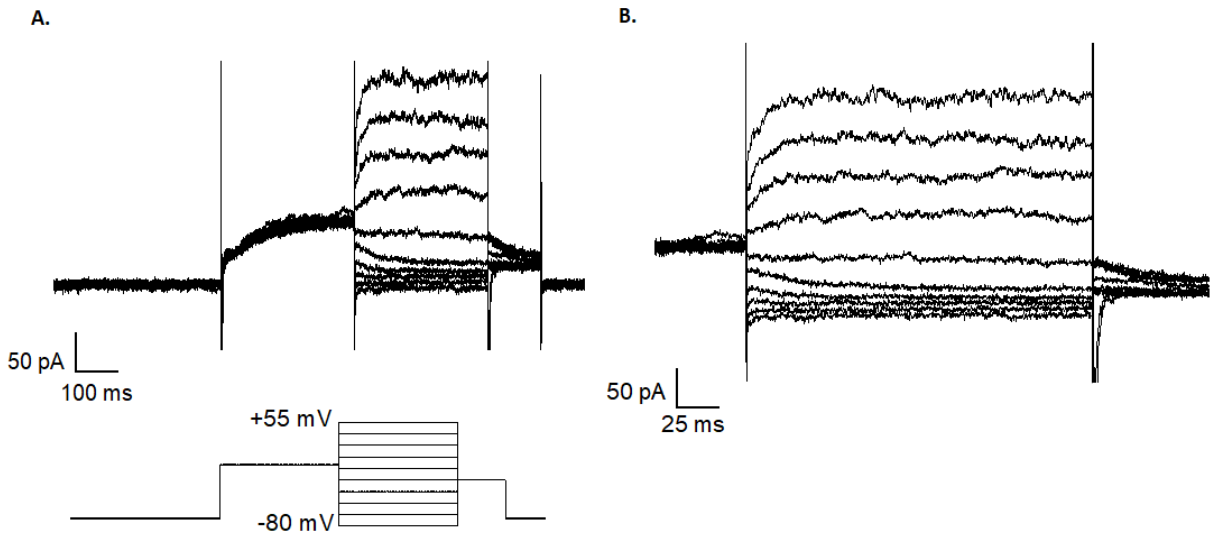


Figure 19: *A.* Endogenous currents from N2a cells with protocol 1. A depolarizing pulse of 0 mV was used to inactivate the fast activating channels, which was followed by test pulses from -80 mV to +55 mV. *B.* A zoomed view of the delayed rectifier current traces shown in *A*.

The electrophysiological parameters of the cells are shown in Table 1.

Table 1: The values of the electrophysiological parameters (*n=9*).

| | $R_e(M\Omega)$ | $R_{seal}$ $(M\Omega)$ | $C_m$ (pF) | $V_{rest}(mV)$ | $R_s$ (MΩ) | $R_{in}(G\Omega)$ |
|---|---|---|---|---|---|---|
| Cell 1 | 4 | 2 | 22 | -15 | 16 | 1.1 |
| Mean | 5.2 | 4.7 | 20.9 | -18.8 | 24.2 | 1.4 |
| Standard Deviation | 0.73 | 2.4 | 4.4 | 7.1 | 12.9 | 0.8 |
| Median | 5.3 | 4 | 22 | -18.7 | 18 | 1.1 |

Figure 20 *A* shows the I-V relation of Cell 1, along with the I-V relation with mean current densities of all the cells with error bars. Figure 20 *B* shows the $g/g_{max}$ of the mean conductances as a function of $V_m$ with Boltzmann fit.

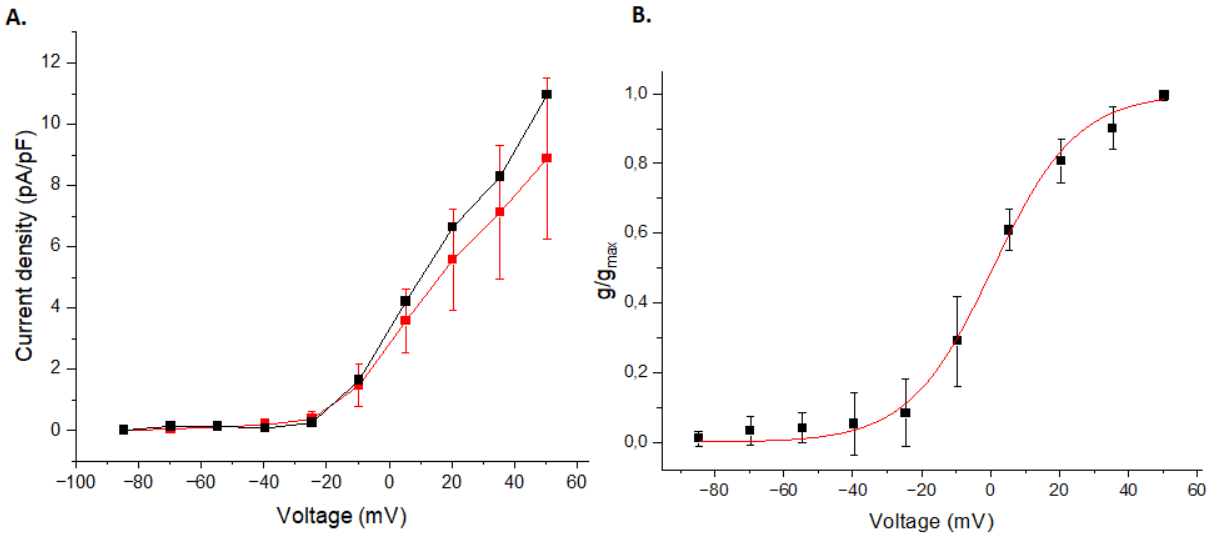


Figure 20: *A.* The steady state I-V relation of the delayed rectifier of Cell 1 (black) and I-V relation with mean current densities with error bars (red, *n=9*). *B.* $g/g_{max}$ as a function of $V_m$ with Boltzmann fit (*n=9*). $V_{1/2} = 0.75 \pm 5.85$ mV and the slope factor $k = 12.68 \pm 2.52$.

The seal was relatively low during the recording of Cell 1, 2 GΩ. However, the $R_s$ was good in comparison to the mean value. The $C_m$, $V_{rest}$ and $R_{in}$ are close to the mean values and, as is observed, the I-V relation fits well within the error bars.

Figure 21 shows the current traces of the delayed rectifier, recorded from Cell 2 as an example of Group 2. I-V relation of the cell is shown in Figure 22, along with the I-V relation of the mean current densities.

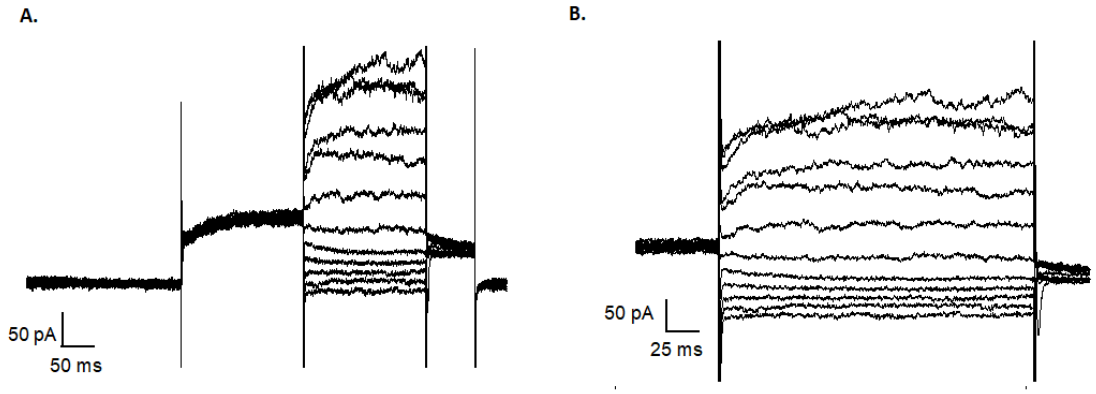


Figure 21: *A.* Endogenous currents from N2a cells with protocol 1, with $V_c$ from -80 mV to +85 mV. *B.* A zoomed view of the delayed rectifier current traces shown in *A*.

The electrophysiological parameters of Cell 2 are presented in Table 2.

Table 2: The values of the electrophysiological parameters ($n$=7).

| | $R_e(M\Omega)$ | $R_{seal}$ $(M\Omega)$ | $C_m$ (pF) | $V_{rest}(mV)$ | $R_s$ $(M\Omega)$ | $R_{in}(G\Omega)$ |
|---|---|---|---|---|---|---|
| Cell 2 | 4.9 | 2 | 24 | -18.4 | 33 | 1 |
| Mean | 4.9 | 2.4 | 21.3 | -24.5 | 23 | 1.6 |
| Standard Deviation | 0.56 | 1.4 | 3.1 | 10.3 | 8.7 | 0.3 |
| Median | 4.9 | 2 | 23 | -23.5 | 20 | 1.7 |

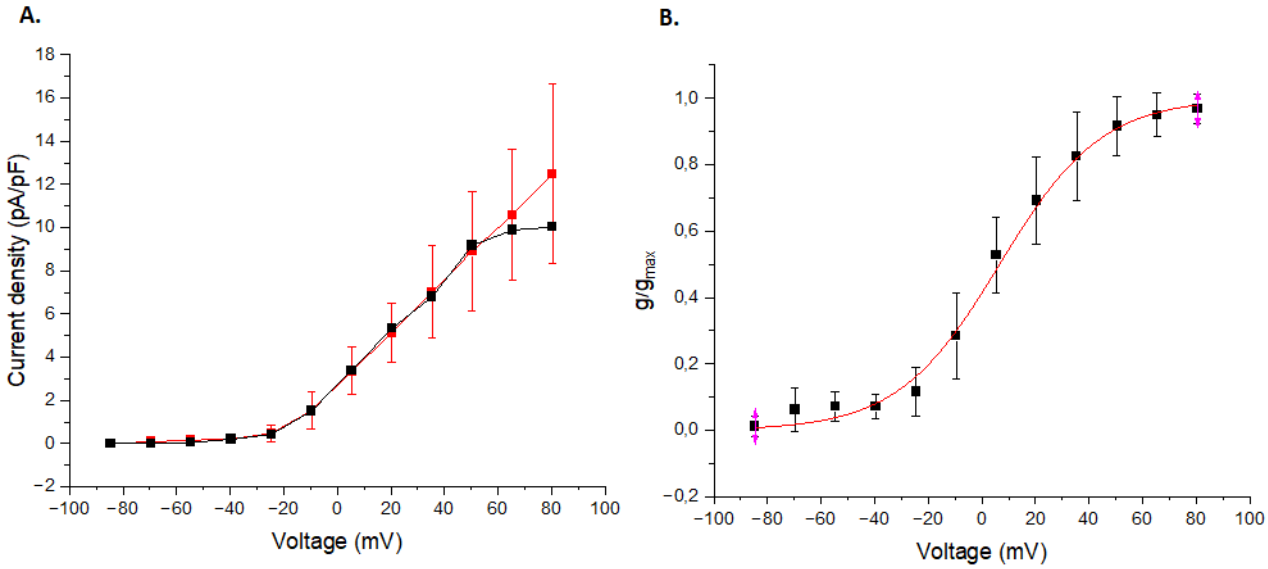


Figure 22: *A.* The steady state I-V relation of the delayed rectifier of Cell 2 (black) and I-V relation with mean current densities with error bars (red, $n$=7). *B.* $g/g_{max}$ as a function of $V_m$ with Boltzmann fit ($n$=7). The mean $V_{1/2}$ = 8.26 $\pm$ 9.66 mV and $k$ = 16.78 $\pm$ 4.18.

The electrophysiological parameters for Cell 2 are close to the mean values, except for the more depolarized $V_{rest}$ and $R_s$, which is higher. Based on the I-V relation, it seems like the $R_s$ has increased during the recording, explaining the lower current densities at +65-80 mV.

The activation of the delayed rectifier was observed approximately between -20 and -10 mV and the conductance increases with depolarization. Table 3 and Table 4 show the mean values of $V_{1/2}$ and slope factor $k$, respectively, for both groups. The box plots presenting the deviation of $V_{1/2}$ and $k$ are shown in Figure 23.

Table 3: The values of $V_{1/2}$.

| | Group 1 ($n$ = 9) | Group 2 ($n$ = 7) |
|---|---|---|
| Mean | 0.75 | 8.26 |
| Standard Deviation | 5.85 | 9.66 |
| Median | 1.25 | 4.05 |

Table 4: The slope factor $k$.

| | Group 1 ($n$ = 9) | Group 2 ($n$ = 7) |
|---|---|---|
| Mean | 12.68 | 16.78 |
| Standard Deviation | 2.52 | 4.18 |
| Median | 13.19 | 17.46 |

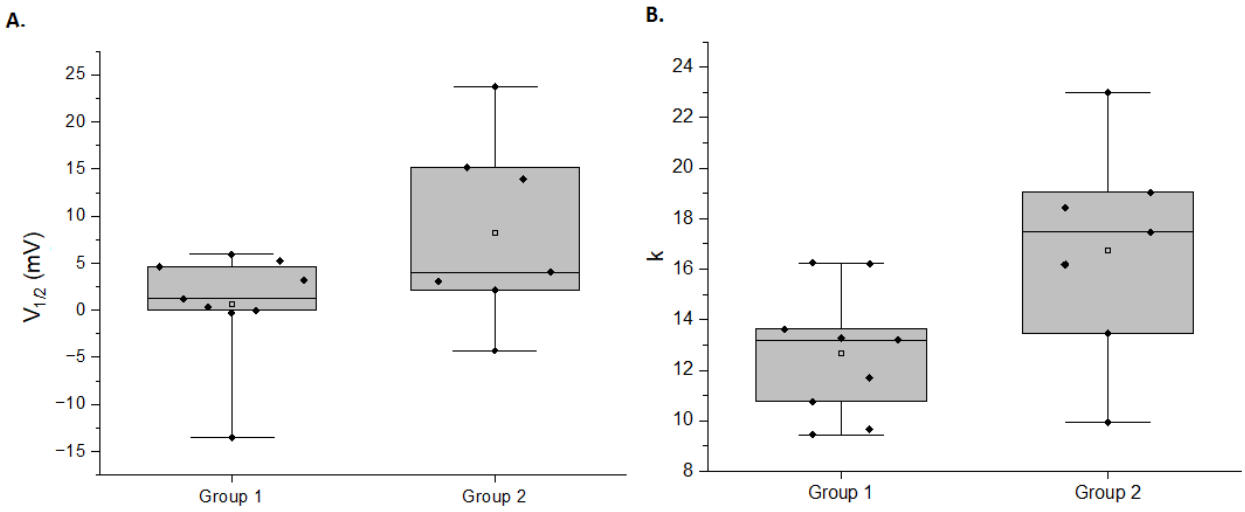


Figure 23: Box charts for Group 1 ($n$=9) and Group 2 ($n$=7) showing the variation of the $V_{1/2}$ ($A$) and the slope factor $k$ ($B$).

In Group 1, there is not much variation between the data points of $V_{1/2}$, except for the one outlier. In contrast, Group 2 shows more deviation. The causes for the deviation are difficult to assess, but it may be a result of a poor signal-to-noise ratio due to a low level of expression of ion channels.

### Effect of $R_s$

Table 5 shows the voltage error, $\Delta V = R_s I_m$, caused by the largest $R_s$ that occurred during the recordings, after 80% compensation. As an example is a cell with the largest current amplitudes.

Table 5: The effect of $R_s$ with the maximum current amplitude of 489 pA at +55 mV. The residual $R_s$ = 52 MΩ · 0.2 = 10.4 MΩ.

| $I_m$ (pA) | $V_m = V_c - V_{ljp}$ (mV) | $\Delta V$ (mV) | $V_m - \Delta V$ (mV) |
|---|---|---|---|
| 0.021 | -84.6 | 0.0002 | -84.60 |
| 1.869 | -69.6 | 0.019 | -69.62 |
| 1.467 | -54.6 | 0.015 | -54.62 |
| 2.035 | -39.6 | 0.021 | -39.62 |
| 4.920 | -24.6 | 0.051 | -24.65 |
| 73.667 | -9.6 | 0.766 | -10.37 |
| 210.047 | 5.4 | 2.185 | 3.22 |
| 306.141 | 20.4 | 3.184 | 17.22 |
| 402.274 | 35.4 | 4.184 | 31.22 |
| 489.323 | 50.4 | 5.089 | 45.31 |

The results show that the largest $\Delta V$ that occurs is about 5 mV. Given the fact that this value is calculated using the largest possible values for $I_m$ and $R_s$, indicates that the effect of $R_s$ is not significant in terms of $\Delta V$ in this experiment.

Table 6 shows the effect of $R_s$ of the same cell, when the $R_s$ decreased from $52M\Omega$ to $18M\Omega$ during the recordings.

Table 6: The same protocol recorded of the same cell with different values of $R_s$. The residual resistance after 80% compensation is $R_{s1} = 52M\Omega \cdot 0.2 = 10.4M\Omega$, whereas $R_{s2} = 18M\Omega \cdot 0.2 = 3.6M\Omega$

| $I_1$ (pA) | $\Delta V$ (mV) | $V_m - \Delta V$ (mV) |
|---|---|---|
| -0.91 | -0.01 | -84.59 |
| -0.34 | -0.004 | -69.60 |
| 0.41 | 0.004 | -54.60 |
| 2.2 | 0.02 | -39.62 |
| 0.56 | 0.01 | -24.61 |
| 12.20 | 0.13 | -9.73 |
| 33.59 | 0.35 | 5.05 |
| 56.01 | 0.58 | 19.82 |
| 76.33 | 0.79 | 34.61 |
| 97.10 | 1.00 | 50.40 |

| $I_2$ (pA) | $\Delta V$ (mV) | $V_m - \Delta V$ (mV) |
|---|---|---|
| 1.65 | 0.02 | -84.62 |
| 6.33 | 0.07 | -69.67 |
| 3.85 | 0.04 | -54.64 |
| 1.01 | 0.01 | -39.61 |
| 0.1 | 0.00 | -24.60 |
| 9.14 | 0.10 | -9.70 |
| 36.54 | 0.38 | 5.02 |
| 65.34 | 0.68 | 19.72 |
| 85.56 | 0.89 | 34.51 |
| 112.84 | 1.20 | 50.20 |

It is observed that with such small currents, the effect of $R_s$ is negligible, at least in terms of voltage-error, when compensation is used. In addition, the effect of $R_s$ on voltage-clamp speed does not introduce a meaningful source of error, when recording slowly activating delayed rectifier steady state currents.

## Eag

The expression of Eag currents was studied using protocol 3. The current traces of Cell 1 are shown as an example in Figure 24 and the electrophysiological parameters of the cells are given in Table 7.

Table 7: The electrophysiological parameters ($n$=3).

| | $R_e(M\Omega)$ | $R_{seal}$ $(M\Omega)$ | $C_m$ (pF) | $V_{rest}(mV)$ | $R_s$ (MΩ) | $R_{in}(G\Omega)$ |
|---|---|---|---|---|---|---|
| Cell 1 | 4.4 | 2 | 18 | -35 | 10 | 2.1 |
| Cell 2 | 5 | 3 | 16 | -14 | 22 | 0.5 |
| Cell 3 | 6 | 2 | 25 | -5 | 22 | 0.82 |
| Mean | 5.1 | 2.3 | 19.7 | -18.0 | 18.0 | 1.15 |
| Standard deviation | 0.81 | 0.58 | 4.7 | 15.4 | 6.9 | 0.83 |
| Median | 5 | 2 | 18 | -14 | 22 | 0.8 |

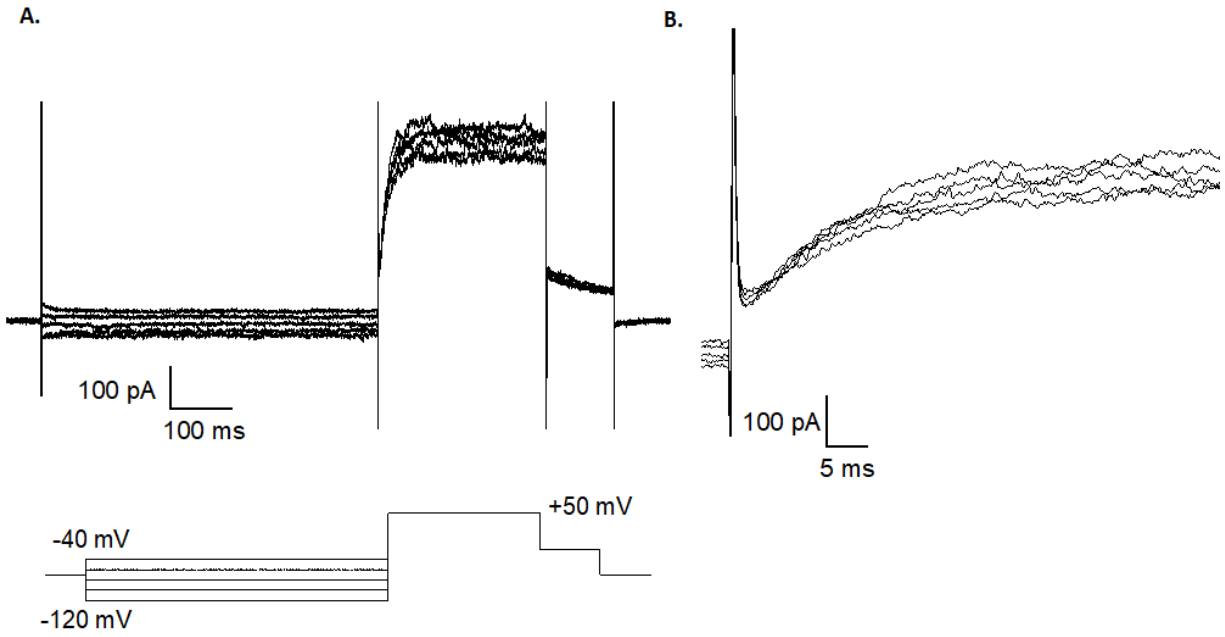


Figure 24: *A.* The current traces with varying $V_c$ from -120 mV to -40 mV. *B.* A zoomed view of the current traces shown in *A*.

It is observed that there is no significant difference between the current traces, even though the voltage pulses preceding the activating voltage pulse vary from -120 mV to -40 mV. Based on these experiments and previous studies, the currents are most likely mediated by Kv2.1. However, to confirm that, it should be studied more specifically, for example with the use of pharmacological tools. On the other hand, Cell 1 expressed the most hyperpolarized $V_{rest}$ of -35 mV, and typically,

it has found to be more hyperpolarized in cells expressing Eag channels, as is shown by Immonen et al. in [54]. This thus implies that these cells do not express Eag channels. However, that can not be confirmed based on these experiments.

### Erg tail current

The Erg-mediated inward tail currents were observed with protocol 4, at a hyperpolarizing voltage pulse of -120 mV ($n$=*1*), as shown in Figure 25. For this experiment, 35 mM of extracellular NaCl was replaced with KCl, in order to modify the driving force of $K^+$. Due to a higher $[K^+]_o$, the Erg-mediated influx of $K^+$ can be observed. The electrophysiological parameters of the cell are given in Table 8.

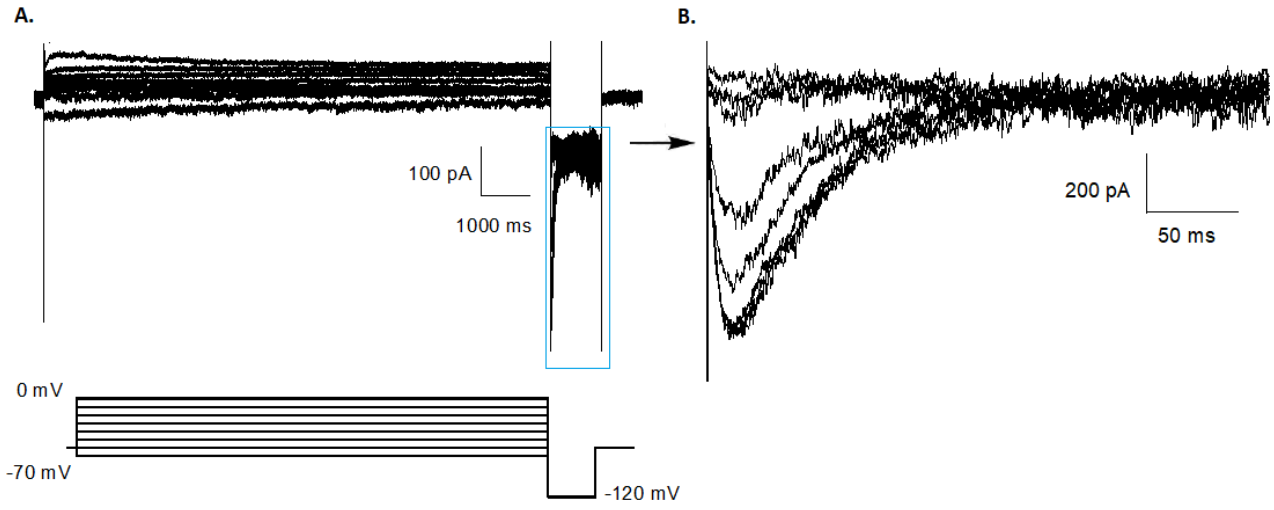


Figure 25: *A*. The current traces with varying $V_H$ from -70 mV to 0 mV. *B*. Erg-mediated tail currents at -120 mV. Recording was done with extracellular solution containing 42.5 mM KCl.

Table 8: The electrophysiological parameters of the cell.

| $R_e$ (MΩ) | $R_{seal}$ (GΩ) | $C_m$ (pF) | $V_{rest}$ (mV) | $R_s$ (MΩ) | $R_{in}$ (GΩ) |
|---|---|---|---|---|---|
| 4.3 | 3 | 22 | -13 | 7 | 0.75 |

The I-V relation of the peak tail currents is shown in Figure 26 *A* and the graph of the normalized currents is shown in Figure 26 *B*.

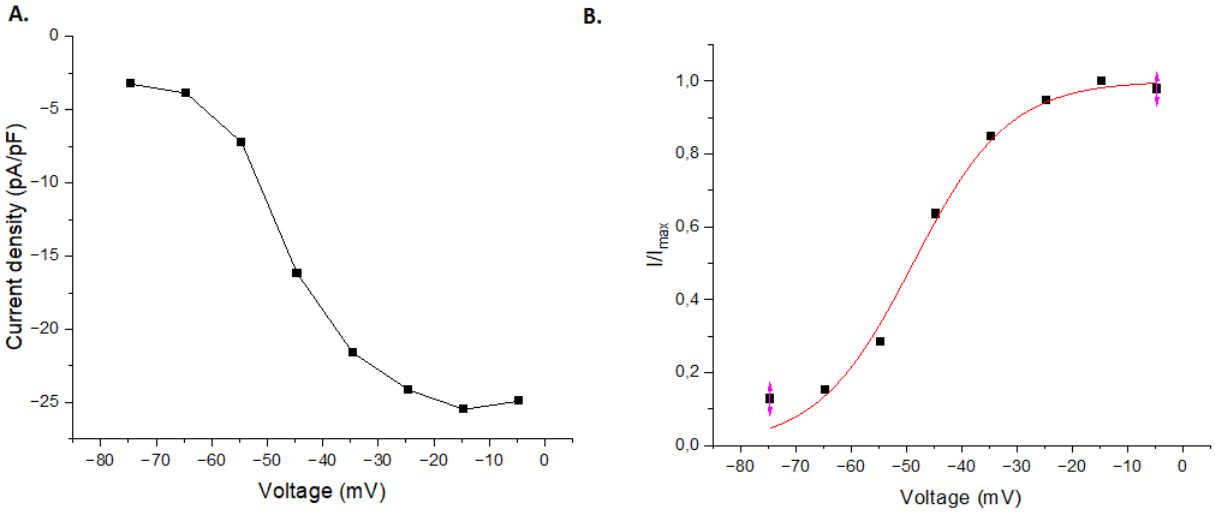


Figure 26: *A.* The peak current densities as a function of $V_c$ at -120 mV. *B.* $I/I_{max}$ of the tail currents with Boltzmann fit. $V_{1/2}$ = -48.73 mV, $k$ = 8.64.

The amplitude of the Erg-mediated tail current increases with depolarizing $V_c$ and the peak current amplitude can be observed with a -15 mV pre-pulse. This recording was only done with one cell to check the expression of the Erg channel in N2a cells. It can, however, be assumed that the tail currents are mediated by Erg, due to the unique kinetics of the channel, that were only observed under specific circumstances.

## 4.2 Nav currents

The current traces recorded with protocol 2 from one cell, expressing distinct Nav currents, are shown as an example in Figure 27 *A*. Figure 27 *B* shows the fast activating and inactivating Nav currents. It can be observed that both activation and inactivation of Nav channels happen within a few milliseconds. The electrophysiological parameters of the cell are shown in Table 9.

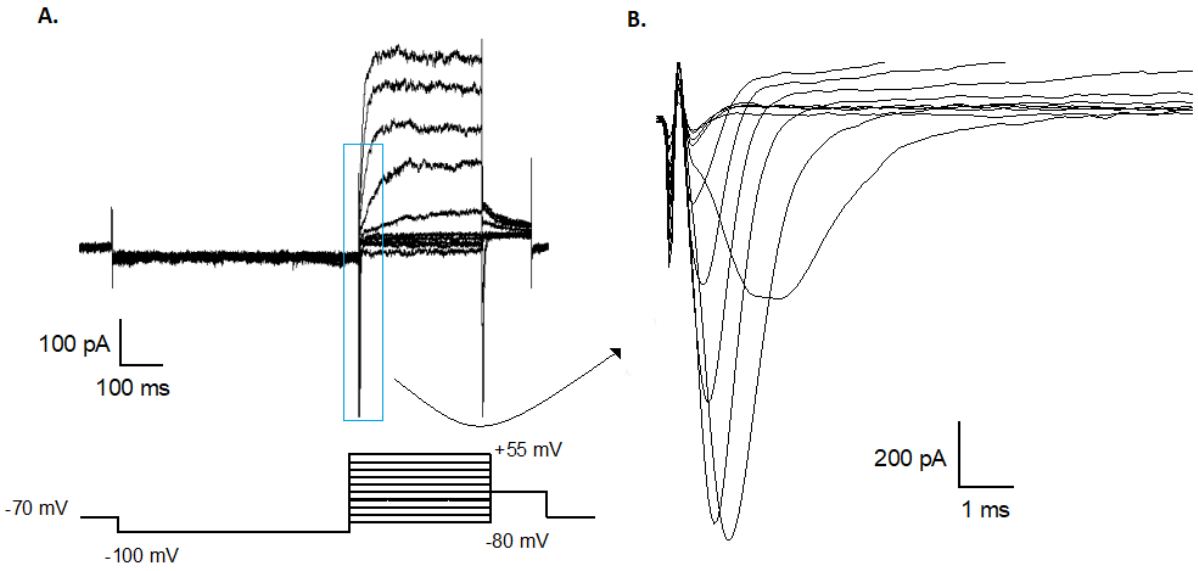


Figure 27: *A*. Current traces recorded with protocol 2. A hyperpolarizing prepulse of -100 mV was followed by test pulses from -80 mV to +55 mV with 15 mV increments. *B*. A zoomed view of Nav currents.

Table 9: The electrophysiological parameters of the recorded cell.

| $R_e$ (MΩ) | $R_{seal}$ (GΩ) | $C_m$ (pF) | $V_{rest}$ (mV) | $R_s$ (MΩ) | $R_{in}$ (GΩ) |
|---|---|---|---|---|---|
| 5 | 4 | 23 | -26 | 25 | 1.75 |

The current traces in Figure 27 are from a cell with significantly larger current amplitudes than any other cell expressed. The difference compared to other cells may be a result of a more differentiated cell and an increased ion channel activity. The mean electrophysiological parameters of the cells are shown in Table 10. Compared to the mean values, it is seen that the seal is slightly better than the mean value. $V_{rest}$ is also a bit more hyperpolarized. On the other hand, $R_s$ and $R_{in}$ are very close to the mean values. Figure 28 shows the comparison of the current densities of the cell shown in Figure 27 and the mean amplitudes with error bars.

Table 10: The mean electrophysiological parameters of the cells (*n=11*).

| | $R_e$ (MΩ) | $R_{seal}$ (GΩ) | $C_m$ (pF) | $V_{rest}$ (mV) | $R_s$ (MΩ) | $R_{in}$ (GΩ) |
|---|---|---|---|---|---|---|
| Mean | 5.1 | 3.4 | 19.8 | -18.1 | 22.5 | 1.6 |
| Standard Deviation | 0.74 | 1.7 | 4.3 | 7.17 | 6.8 | 0.6 |
| Median | 5 | 3 | 22 | -18.7 | 20 | 1.5 |

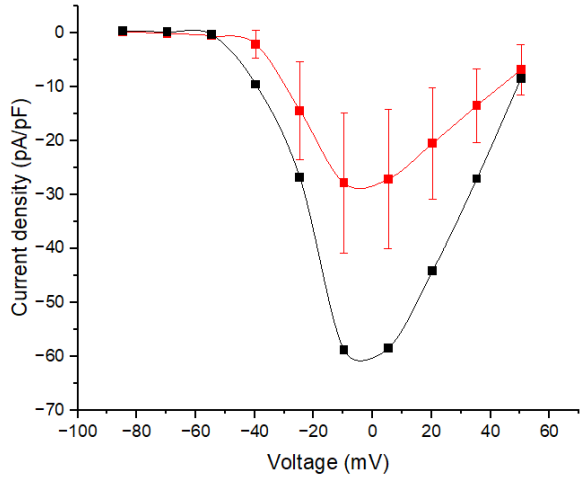


Figure 28: I-V relation of mean current amplitudes with error bars (red, *n=11)* and the I-V relation of the cell shown in Figure 27 (black).

Figure 29 *A* shows the $g/g_{max}$ plotted against $V_m$ with Boltzmann fit for the cells recorded with $V_c$ from -80 mV up to +55 mV. In Figure 29 *B*, the corresponding graph is shown for recordings with $V_c$ up to +70 mV. The values for $V_{1/2}$ and $k$ are presented in Table 11 and Table 12, respectively.

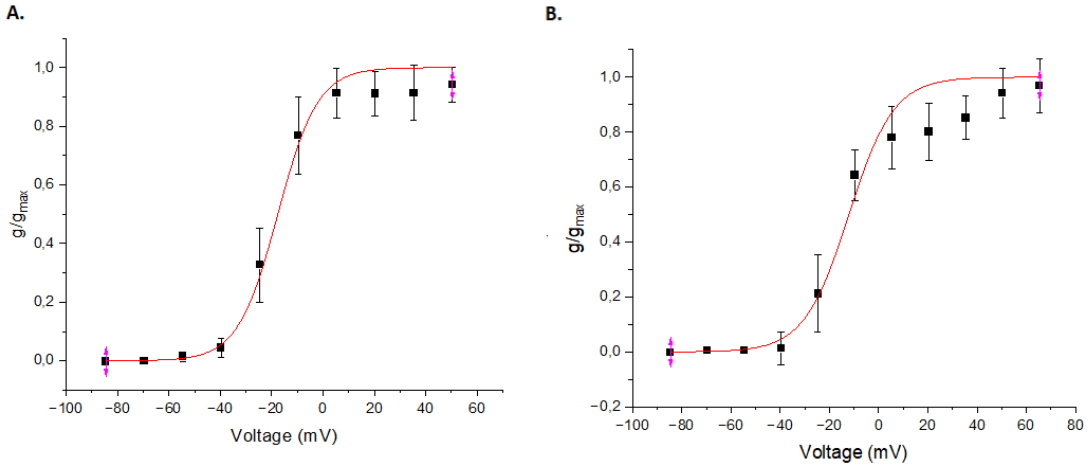


Figure 29: *A*. The normalized conductance curves with Boltzmann fit for recordings with $V_c$ from -80 mV to +55 mV (*n=7)*. $V_{1/2}$ = -17.78 ± 5.46 mV and $k$ = 8.22 ± 2.39. *B*. The normalized conductance curves with Boltzmann fit for recordings with $V_c$ from -80 mV to +70 mV (*n=4)*. $V_{1/2}$ = -12.75 ± 11.22 mV and $k$ = 11.74 ± 5.93.

Table 11: The $V_{1/2}$ of the cells.

| | Group 1 (*n=7*) | Group 2 (*n=4*) |
|---|---|---|
| $V_{1/2}$ | -17.78 | -12.75 |
| Standard Deviation | 5.46 | 11.22 |
| Median | -17.76 | -11.59 |

Table 12: The slope factor $k$ of the cells.

| | Group 1 (*n = 7*) | Group 2 (*n = 4*) |
|---|---|---|
| $k$ | 8.22 | 11.74 |
| Standard Deviation | 2.39 | 5.93 |
| Median | 7.44 | 13.32 |

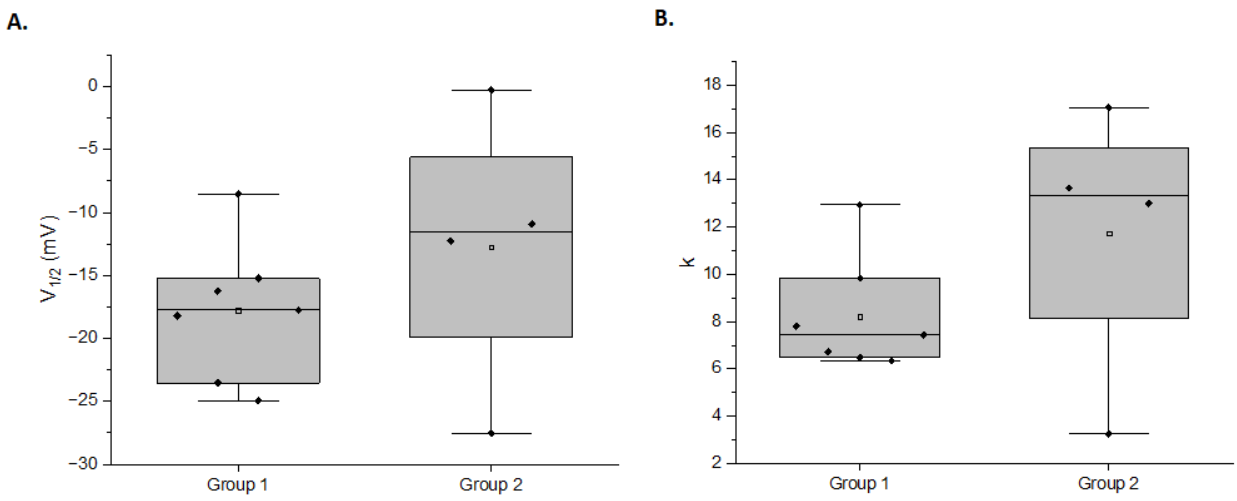


Figure 30: *A.* A box chart showing the variation of the $V_{1/2}$ for Group 1 (*n=7*) and Group 2 (*n=4*). *B.* A box chart showing the variation of the slope factor $k$ for Group 1 (*n=7*) and Group 2 (*n=4*).

The threshold of activation for the fast activating Nav channels was approximately between -50 mV and -40 mV. The peak current amplitude was achieved between -10 and +5 mV. The values of $E_{Na}$ were obtained by extrapolating the I-V relations, and varied from +52 mV to +73 mV. The mean value of $E_{Na}$= +64.1± 7.5 mV is close to the $E_{Na}$ = +64.8 mV reported in [36]. The maximum $g_{max}$ was 25.3 nS. The currents with more depolarized voltages, i.e. +70-85 mV, were difficult to analyse in some recordings, due to the effect of $R_s$ and possible overlapping with Kv currents.

Moreover, the chosen frequency of the Bessel filter of the amplifier, being at 2 kHz results in a temporal resolution of 500 $\mu$s. Considering that the time constant for the activation of the Nav

currents is of the order of 1 ms and even below that, the frequency is too low. As a result, some part of the signal can be distorted and the shape of the peaks of the currents may appear wider. An ideal frequency for the recording of the fast Nav currents is at least 5 kHz, which results in a temporal resolution of 200 $\mu$s.

**Effect of $R_s$**

To estimate the $\Delta V$ caused by $R_s$ in Nav recordings, it is calculated using the maximum current amplitudes that were observed. For Nav currents, the highest current amplitude was -1295.65 pA at $V_m$ = -9.6 mV. The $\Delta V$ caused by $R_s$ in that recording is shown in Table 13. The largest possible $R_s$ in the recordings of Nav currents was 35 MΩ. Thus, the residual $R_s$ = 35MΩ·0.2 = 7 MΩ.

Table 13: The effect of $R_s$ with the maximum current amplitudes and residual $R_s$ of 7 MΩ.

| $I_1$ (pA) | $V_m = V_c - V_{ljp}$ (mV) | $\Delta$V (mV) | $V_m - \Delta V$ (mV) |
|---|---|---|---|
| 5.62 | -84.60 | 0.04 | -84.64 |
| 2.62 | -69.60 | 0.02 | -69.62 |
| -7.93 | -54.60 | -0.06 | -54.54 |
| -211.00 | -39.60 | -1.48 | -38.12 |
| -592.16 | -24.60 | -4.15 | -20.45 |
| -1295.65 | -9.60 | -9.07 | -0.53 |
| -1287.17 | 5.40 | -9.01 | 14.41 |
| -971.68 | 20.40 | -6.80 | 27.20 |
| -596.37 | 35.40 | -4.17 | 39.57 |
| -187.07 | 50.40 | -1.31 | 51.71 |

In this recording, current amplitudes are significantly higher than in any other recording. With the residual $R_s$ of 7 MΩ, the largest $\Delta V$ that occurs is approximately -9 mV at $V_m = -9.6$ mV. It is clearly larger than the $\Delta V$ in the previous recordings. The overall effect of $R_s$ is still not significant in terms of the voltage-error. However, it does affect the voltage-clamp speed, with a time constant according to the equation (44)

$$\tau = R_s C_m,$$

which is important to take into consideration when recording the fast activating Nav currents.

## 4.3 Voltage-sensitive currents in the voltage-range of $E_{Cl}$

The endogenous currents were studied with voltage protocol 5, between voltages from -100 mV to 0 mV in order to study the suitability of the N2a cell line for $E_{Cl}$ recordings. A total of seven cells were recorded, and the corresponding electrophysiological parameters are given in Table 14.

Table 14: Basic electrophysiological properties of the cells for assessing N2a suitability for $E_{Cl}$ recordings.

| | $R_e$ (MΩ) | $R_{seal}$ (GΩ) | $V_{rest}$ (mV) | $C_m$ (pF) | $R_s$ (MΩ) | $R_{in}$ (GΩ) |
|---|---|---|---|---|---|---|
| Cell 1 | 4 | 1 | -38 | 24 | 20 | 1.7 |
| Cell 2 | 5 | 2 | -18.1 | 21 | 19 | 1.15 |
| Cell 3 | 4.9 | 1 | -18.4 | 24 | 35 | 1 |
| Cell 4 | 4.4 | 2 | -29.5 | 23 | 17 | 1.55 |
| Cell 5 | 6 | 2 | -5 | 25 | 22 | 0.8 |
| Cell 6 | 4.4 | 2 | -35 | 18 | 15 | 2.1 |
| Cell 7 | 6 | 2 | -32 | 27 | 22 | 0.5 |
| Mean | 4.9 | 1.7 | -25.1 | 23.1 | 21.4 | 1.3 |
| Standard Deviation | 0.79 | 0.49 | 11.8 | 2.9 | 6.5 | 0.56 |
| Median | 4.9 | 2 | -29.5 | 24 | 20 | 1.2 |

There is some variation in the values of $V_{rest}$, which is expected considering the nature of the N2a cells. $R_{seal}$ is in the same range for all recordings, although it could have been better. A higher seal could not be achieved during these recordings, and a possible cause for that could be the condition of the cells.

Typically, this would not be an ideal case when doing whole-cell recordings. When considering the suitability of the cells for $E_{Cl}$ recordings, however, it gives a more realistic result as the recordings are usually done in perforated patch-clamp configuration. During perforated patch-clamp, the use of the pore-forming agents results in a lower seal.

The range of the $R_{in}$ of these cells is also suitable considering the perforated patch-clamp. It is considered necessary to at least have an $R_{in}$ of approximately 400 MΩ or more, as the $R_{in}$ decreases during the recordings due to the pore-forming agents. This is to make sure that the function of the cells would be as close to what it normally is, as possible.

The raw current traces recorded from Cell 4 are shown in Figure 31 *A*. Figure 31 *B.* shows the current traces from the same recording with leak subtraction. The compensation was adjusted to 80%.

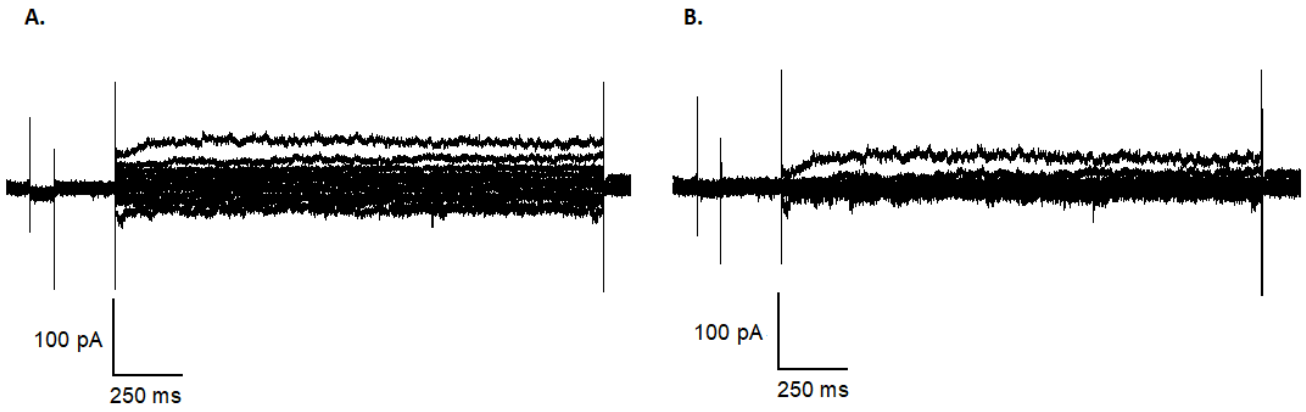


Figure 31: *A.* Raw data of the currents with voltages from -100 mV to 0 mV. *B.* The same currents as in *A*, but with leak subtraction.

Figure 32 shows a comparison of the leak subtracted currents and raw currents plotted against the $V_m$.

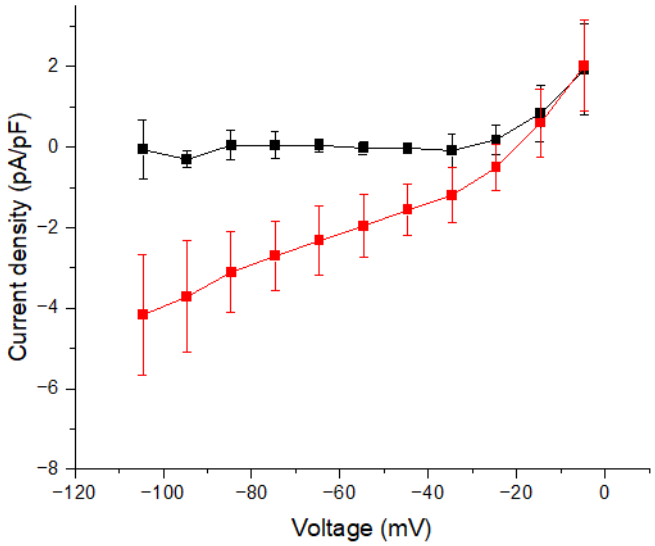


Figure 32: The mean current densities ($n$=7) with leak subtraction (black) and without leak subtraction (red).

Doing the leak subtraction shows that most of the currents are a result of leak channels. The voltage-gated Nav and Kv channels are therefore not contributing significantly to the currents in this voltage-range. Currents of any significance only activate at about -10 mV, which indicates that they are the delayed rectifier currents. That occurs at more depolarized value than what the typical $E_{Cl}$ is. Therefore, these results support the suitability of the N2a cells for the $E_{Cl}$ recordings.

The comparison of recordings with 80% compensation and without compensation is shown in Figure 33. It is observed that the effect of compensation is not significant in these experiments, because the currents are extremely small.

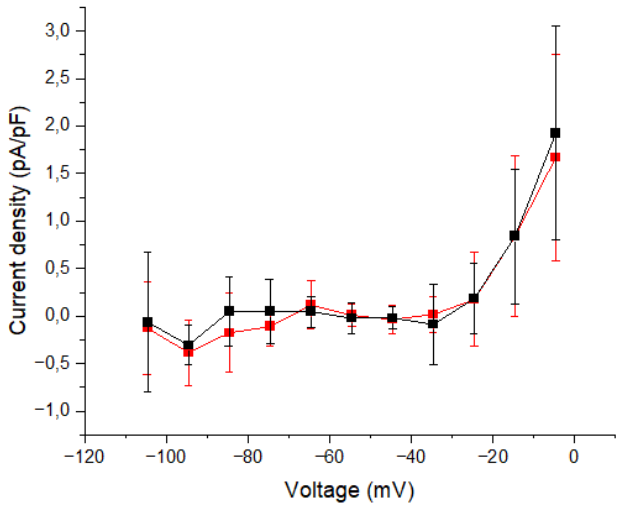


Figure 33: The mean current densities ($n$=7) with 80% compensation (black) and without compensation (red). Leak subtraction is done in both cases.

Figure 34 shows current traces from Cell 5 ($A$) and Cell 6 ($B$) with $R_{in}$ of 0.8 GΩ and 2.1 GΩ, respectively. $R_{in}$ is dependent on the amount of open ion channels and the precision of its estimation is dependent on the $R_{seal}$. It can be seen that Cell 5 shown in Figure 34 $A$ has higher current amplitudes while having a lower $R_{in}$. However, the seal can also affect this. $R_{in}$ is also dependent on the state of differentiation; in a less differentiated cell, $R_{in}$ is typically higher due to a lower expression of ion channels.

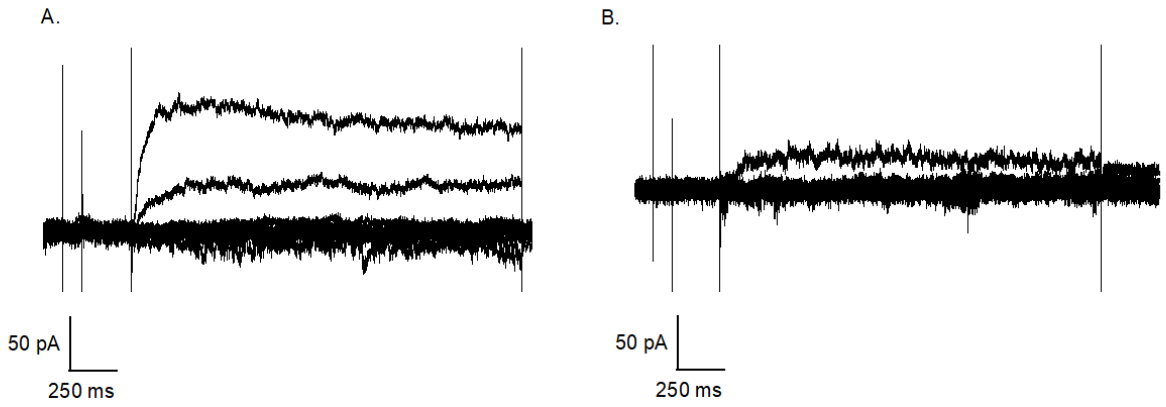


Figure 34: $A$. Current traces of Cell 5 with $R_{in}$ = 0.8 GΩ. $B$. Current traces of Cell 6 with $R_{in}$ = 2.1 GΩ.

To confirm the suitability of the N2a cells for $E_{Cl}$ recordings, it is necessary to compare the cells expressing native currents with those expressing GlyRs, which are commonly used for $E_{Cl}$ recordings. An example of a GPPC recording of a cell expressing wild type KCC2 and GlyRs is shown in Figure 35. In the recording, the reversal potential for the currents is at around -65 mV, being within the range of a typical $E_{Cl}$ recording.

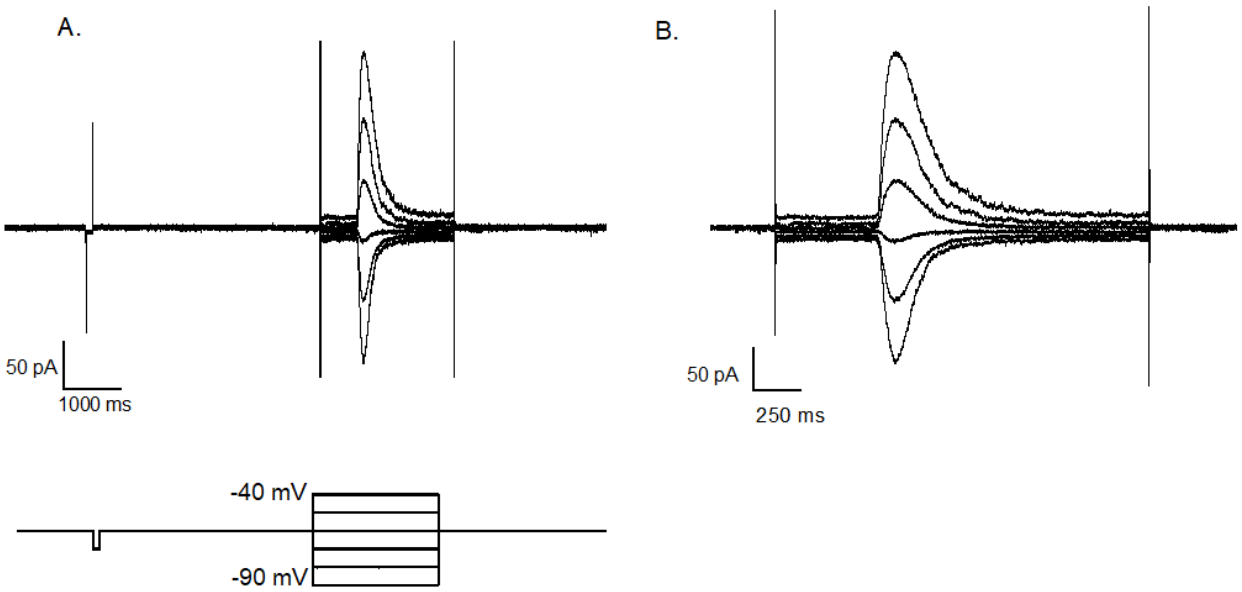


Figure 35: *A.* Preliminary data from $E_{Cl}$ recordings of a cell expressing wild type KCC2 and GlyRs. The currents were induced using a brief pulse of 50 $\mu$M glycine. The recording is the courtesy of Viivi Järvelä. *B.* A zoomed view of the currents in *A*.

Comparing the recording shown in 35 with the recording of the native currents shown in Figure 31, it is seen that the N2a cells do not express such currents that would interfere with the glycine currents, which further supports the suitability of these cells for $E_{Cl}$ recordings.

# 5 Discussion

The experiments done with cultured N2a cells revealed the expression of certain Kv channels as well as fast activating and inactivating Nav channels. These results could be expected, since previous studies have reported mouse neuroblastoma cell lines to express these channels.

The Kv channels that could be distinguished include, presumably Kv2.1, mediating delayed rectifier currents. To confirm this, further studies should be done using pharmacological tools, for example. The activation of the delayed rectifier currents was observed approximately between -20 and -10 mV. The conductance of the delayed rectifier increased with depolarization.

The possible expression of Eag channels was also studied with an activation pulse of +50 mV, which was preceded by varying hyperpolarizing pulses from -120 mV to -40 mV. The resulting currents were small and there was also a relatively high amount of noise, which made the analysis difficult. The currents may as well be mediated by the Kv2.1. A supporting evidence for the currents being mediated by Kv2.1 is the rather depolarized $V_{rest}$ of the recorded cells, since the $V_{rest}$ is typically more hyperpolarized in cells expressing Eag channels. However, to confirm that, further experiments should be done. For more specific experiments studying the expression of Eag channels, the extracellular solution could also be modified by changing the $[Mg^{2+}]$, since the activation slows down with the presence of $Mg^{2+}$.

Additionally, Erg-mediated inward $K^+$ tail currents could be distinguished by increasing $[K^+]_o$, which created the driving force for the influx of $K^+$. There was only one experiment made to confirm the expression of the channel in the N2a cells, and therefore, further analysis of the channel kinetics was not made. However, having such unique kinetics, which could only be observed under certain conditions, indicates that the cell expressed Erg channels.

The fast activating and inactivating Nav currents showed a threshold of activation at about -40 mV, with a preceding hyperpolarizing voltage pulse that removes the inactivation of the channels. For Nav channels, the mean $E_{Na}$ was measured at +64.1 mV, which is close to the value of +64.8 mV that was reported in [36]. The peak current amplitudes of the Nav-mediated currents were observed between -10 mV and +5 mV.

Some of the Nav currents were, however, difficult to analyse especially at more depolarized voltages. This is most likely due to the overlapping with other signals, including currents from fast activating Kv channels, as well as transients due to insufficient compensation. For further experiments of Nav currents, the use of Kv channel blockers could improve the quality of the experiments. The Kv channels expressed in N2a cells are known to be sensitive to TEA, so that could be used, for example. In addition, the frequency of the filter of the amplifier could be increased to 5 kHz, in order to get a better temporal resolution.

The main focus of these experiments was to validate the suitability of the N2a cells for $E_{Cl}$ recordings. The endogenous voltage-gated currents were recorded with a protocol, in which $V_H$ was set to -60 mV and the voltage steps went from -100 mV to 0 mV in 10 mV increments. Overall, the results of these measurements showed that there are mainly leak currents within that voltage range, indicating that the cells would be suitable for $E_{Cl}$ recordings. Even though there are fast activating Nav channels that activate between -50 and -40 mV, they remain in the inactivated state without the removal of inactivation. On the other hand, for the Erg-mediated currents to activate, the specific conditions are needed. Therefore, the Erg currents would not overlap with the currents recorded in $E_{Cl}$ recordings, either.

When it comes to the perforated patch-clamp, it is important for the recorded cells to have an $R_{in}$ of at least 400 MΩ. Therefore, cells of lower passage are typically used for perforated

patch-clamp recordings. The cells used in the present study, with passages of 4-6, seem to have a sufficient $R_{in}$ for that, as the values of $R_{in}$ varied between 0.6 to 2.1 GΩ, supporting the suitability of these cells for $E_{Cl}$ recordings.

Considering the quality of the experiments in general, improvement could be done by increasing the amount of recorded cells, since the amount that was done for this study, was relatively small, although some of the results are also supported by other studies. Additionally, cells of different passage could be included.

The $C_m$ varied from 14 pF to 29 pF and the mean $C_m$ was approximately 21 pF, which is within an expected range. The $V_{rest}$ of the analysed cells was between -4 to -38 mV and the mean value was -21 mV, which is close to the range reported in other studies, even though it is on the more depolarized side. That could indicate the other studies to have more strict quality criteria, compared to the experiments in this thesis. These type of variations can be expected, however, since cells are living organisms and various factors, such as the state of differentiation and the phase of the cell cycle, affect the electrophysiological properties of individual cells.

In some of the experiments, stable seals were difficult to achieve. This is important to take into account, especially when considering the estimation of $V_{rest}$ of the cells. The importance of a good seal has been highlighted, for example by Perkins in [55], in which it is stated that the $R_{seal}$ should be significantly higher than the $R_{in}$, ideally 10 times the $R_{in}$. It is clear that such good seals were not obtained in the experiments done in the present study, which most likely has affected the quality of the voltage-clamp and therefore the estimation of $V_{rest}$, as well as other parameters. This is therefore a disadvantage of the N2a cells considering the perforated patch-clamp experiments, as the high $R_{in}$ in relation to the $R_{seal}$ may cause problems during perforated patch-clamp recordings, distorting the actual voltages the cells experience.

Some variation could be observed in $R_s$ between recordings. It was shown that there was no significant voltage-error due to the $R_s$, since the recorded currents were so small. However, it did affect the speed of the voltage-clamp. This is important to consider especially in the experiments recording the fast Nav currents. In addition, the quality of the compensation was not sufficient in all the recordings, and was therefore considered when choosing the cells for the analysis. The theoretical LJP between the used solutions was 4.6 mV, and it was taken into account in the analysis, as it always affects the results.

The values of $R_e$ were stable throughout the recordings, between 4-6 MΩ, which is a typical range in whole-cell patch-clamp. Possible improvements for the pipettes could be done using coatings of hydrophobic substances, which may help to prevent the bath solution from creeping up the pipette, and therefore reduce noise. Moreover, fire-polishing the pipettes could be considered, since it has been found to help seal formation and the quality of the seal, in some cases.

# 6 References

[1] Johnston D., Wu S., Foundations of cellular neurophysiology (1995)

[2] Purves D. et al., Neuroscience Fourth Edition, Sinauer Associates Inc., 46-176 (2008)

[3] Hille B., Ion Channels of Excitable Membranes, Third Edition, Sinauer Associates Inc. (2001)

[4] Medina I., Friedel P., Rivera C., Kahle K., Kourdougli N., Uvarov P., Pellegrino C., Current view on the functional regulation of the neuronal K-Cl cotransporter KCC2, Frontiers in Cellular Neuroscience (2014), doi: 10.3389/fncel.2014.00027

[5] Medina I., Pisella L. I., Methods for investigating the activities of neuronal chloride transporters, Neuronal Chloride Transporters in Health and Disease, Academic Press, 21-41 (2020)

[6] Barbour B., Electronics for electrophysiologists (2014)

$https://www.biologie.ens.fr/\ barbour/electronics_for_electrophysiologists.pdf$

[7] Schwiening C. J., A Brief Historical Perspective: Hodgkin and Huxley, Journal of Physiology, 590, 2561-2575 (2012, doi: 10.1113/jphysiol.2012.230458

[8] Multiclamp 700B manual

$https://neurophysics.ucsd.edu/Manuals/Axon$

[9] Molecular Devices, The Axon Guide, 3rd edition (2012)

[10] Berman J. M., Awayda M. S., Redox artifacts in electrophysiological recordings, American Journal of Physiology, 304 (2013)

https://www.ncbi.nlm.nih.gov/pmc/articles/PMC3625719/

[11] Series Resistance Compensation

$https://swharden.com/blog/2020-10-11-model-neuron-ltspice/Drexel_Gao_Lab_Series_Resistance_Compensation.pdf$

[12] Jérome Montnach et. al., Computer modeling of whole-cell voltage-clamp analyses to delineate guidelines for good practice of manual and automated patch-clamp, Scientific Reports 11 (2021)

$https://www.nature.com/articles/s41598-021-82077-8$

[13] Electrophysiology Measurements for Studying Neural Interfaces, Elsevier (2020)

https://doi.org/10.1016/B978-0-12-817070-0.00006-3

[14] Martinez A. H., Mohiuddin S. S., Biochemistry, Chloride Channels, StatPearls Publishing (2022)

[15] Mahadevan V., Woodin M. A., Regulation of neuronal chloride homeostasis by neuromodulators, The Journal of Physiology, 594, 2593-2605 (2016), doi: 10.1113/JP271593

[16] Rahmati N., Hoebeek F. E., Peter S., De Zeeuw C. I., Chloride Homeostasis in Neurons With Special Emphasis on the Olivocerebellar System: Differential Roles for Transporters and Channels, Frontiers Cellular Neuroscience, Vol. 12 (2018)

https://doi.org/10.3389/fncel.2018.00101

[17] Virtanen M. A., Uvarov P., Mavrovic M. et al., The Multifaceted Roles of KCC2 in Cortical Development, Trends in Neurosciences, Vol. 44, 5, 378-392 (2021)

https://doi.org/10.1016/j.tins.2021.01.004

[18] Wright R., Newey S. E., Ilie A., et al., Neuronal Chloride Regulation via KCC2 is Modulated Through a $GABA_B$ Receptor Protein Complex, Journal of Neuroscience, 37, 5447-5462 (2017), doi: 10.1523/JNEUROSCI.2164-16.2017

[19] Liu R., Wang J., Liang S., Zhang G., Yang X., Role of NKCC1 and KCC2 in Epilepsy: From Exrpession to Function, Frontiers in Neurology (2019), doi: 10.3389/fneur.2019.01407

[20] Blaesse P., Airaksinen M. S., Rivera C., Kaila K., Cation-Chloride Cotransporters and Neuronal Function, Cell Press (2009), DOI 10.1016/j.neuron.2009.03.003

[21] Watanabe M., Fukuda A., Development and regulation of chloride homeostasis in the central nervous system, Frontiers Cell. Neurosci., Vol. 9 (2015)

https://doi.org/10.3389/fncel.2015.00371

[22] Goutierre M., Awabdh S., Donneger F., Francois E. et al., KCC2 Regulates Neuronal Excitability and Hippocampal Activity via Interaction with Task-3 Channels, Cell Reports, Vol. 28, 91-103 (2019)

https://doi.org/10.1016/j.celrep.2019.06.001

[23] Acton B. A., Mahadevan V. et al., Hyperpolarizing GABAergic Transmission Requires the KCC2 C-Terminal ISO Domain, The Journal of Neuroscience, 8746-8751 (2012), doi: 10.1523/JNEUROSCI.6089-11.2012

[24] Zhu G., Zhang Y., Xu H., Jiang C., Identification of endogenous outward currents in the human embryonic kidney (HEK293) cell line, Journal of Neuroscience Methods, Vol 81, 73-83 (1998)

*https://www.sciencedirect.com/science/article/abs/pii/S0165027098000193?via*

[25] Trapani J. G., Korn S. J., Control of ion channel expression for patch clamp recordings using an inducible expression system in mammalian cells, BMC Neuroscience (2003), doi: 10.1186/1471-2202-4-15

[26] Hasan Md. Mahadhi et al., Transfection methods for high-throughput cellular assays of voltage-gated calcium and sodium channels involved in pain, PLOS One (2021)

https://doi.org/10.1371/journal.pone.0243645

[27] Chong Z., Yeap S., Ho W., Transfection types, methods and strategies: a technical review, Peer J (2021), doi: 10.7717/peerj.11165

[28] Ponce A., Castillo A., Hinojosa L., Martinez-Rendon J., Cereijido M., The expression of endogenous voltage-gated potassium channels in HEK293 cells is affected by culture conditions, Physiological Reports Vol. 6 (2018)

*https://physoc.onlinelibrary.wiley.com/doi/pdfdirect/*10.14814/*phy*2.13663

[29] Ooi A. et al., A Guide to Transient Expression of Membrane Proteins in HEK-293 Cells for Functional Characterization, Frontiers in Physiology, Vol. 7 (2016), DOI: 10.3389/fphys.2016.00300

[30] Meyer R., Heinemann S., Characterization of an eag-like potassium channel in human neuroblastoma cells, Journal of Physiology, 49-56 (1998), DOI: 10.1111/j.1469-7793.1998.049br.x

[31] Martin E., Gandawijaya J., Oguro-Ando A., A Novel Method for Generating Glutamatergic SH-SY5Y Neuron-Like Cells Utilizing B-27 Supplement, Frontiers in Pharmacology (2020)

https://doi.org/10.3389/fphar.2022.943627

[32] Rogers M., Zidar N et al., Characterization of Endogenous Sodium Channels in the ND7-23 Neuroblastoma Cell Line: Implications for Use as a Heterologous Ion Channel Expression System Suitable for Automated Patch Clamp Screening, Assay Drug Dev Technol. 14, 109-130 (2016)

doi: 10.1089/adt.2016.704

[33] Lee J., Kim S., Kim H., Kim H. J., Yu F., Nav1.6 and Nav1.7 channels are major endogenous voltage-gated sodium channels in ND7/23 cells, PLoS One 14 (2019)

https://doi.org/10.1371/journal.pone.0221156

[34] Wu P.-M., Cho H.-Y., Chiang C.-W. et al., Characterization in Inhibitory Effectiveness of Carbamazepine in Voltage-Gated $Na^+$ and Erg-mediated $K^+$ Currents in a Mouse Neural Crest-Derived (Neuro-2a) Cell Line, International Journal of Molecular Sciences, 23 (2022)

https://doi.org/10.3390/ijms23147892

[35] Tremblay R. G., Sikorska M., et al., Differentiation of Mouse Neuro 2A Cells into Dopamine Neurons, Journal of Neuroscience Methods, Vol. 186, 60-67 (2010)

https://doi.org/10.1016/j.jneumeth.2009.11.004

[36] Iwata M., Komori S., Unno T., Minamoto N. and Ohashi H., Modification of Membrane Currents in Mouse Neuroblastoma Cells Following Infection with Rabies Virus, British Journal of Pharmacology, 126, 1691-1698 (1999)

[37] Chiba O., Shimada N., Yoshio S., Kudo Y. et al., State-Dependent Inhibition of Voltage-Gated Sodium Channels in Neuroblastoma Neuro-2A Cells by Arachidonic Acid from *Halichondria okadai*, Chemical Research in Toxicology, 35, 1950-1961 (2022)

[38] Grizel A. V., Glukhov G. S. and Sokolova O. S., Mechanisms of activation of voltage-gated potassium channels, Acta Naturae, Vol. 6, 10-26 (2014)

*https* : *//www.ncbi.nlm.nih.gov/pmc/articles/PMC*4273088/

[39] Chao C.-C., Shieh J., Kuo S.-C. et al., HMJ-53A Accelerates Slow Inactivation Gating of Voltage-Gated $K^+$ Channels in Mouse Neuroblastoma N2A Cells, Neuropharmacology, Vol. 54, 7, 1128-1135 (2008)

[40] Barros F. et al., The EAG Voltage-Dependent K+ Channel Subfamily: Similarities and Differences in Structural Organization and Gating, Frontiers in Pharmacology, Vol 11 (2020)

doi: 10.3389/fphar.2020.00411

[41] Codding S. J., Johnson A. A., Trudeau M. C., Gating and regulation of KCNH (ERG, EAG and ELK) channels by intracellular domains, Channels, Vol. 14, 294-309 (2020)

https://doi.org/10.1080/19336950.2020.1816107

[42] Liu Q., Trudeau M. C., Eag domains Regulate LQT Mutant hERG Channels in Human Induced Pluripotent Stem Cell-Derived Cardiomyocytes, Plos One (2015)

https://doi.org/10.1371/journal.pone.0123951

[43] Whicher J. R., MacKinnon R, Regulation of Eag1 by its Intracellular Domains, eLife (2019)

*https* : *//elifesciences.org/articles/*49188#*s*2

[44] Vandenberg J. et al., hERG $K^+$ channels: structure, function and clinical significance, Physiological Reviews 92, 1393-1478 (2012)

doi:10.1152/physrev.00036.2011

[45] Alonso-Ron, Carlos et al., Thermodynamic and Kinetic Properties of Amino-Terminal and S4-S5 Loop HERG Channel Mutants under Steady-State Conditions, Biophysical Journal, Vol. 94, 3893-3911 (2008)

doi: 10.1529/biophysj.107.116731

[46] Subbiah R. N., Clarke C. E. et al., Molecular basis of slow activation of the human ether-á-go-go related gene potassium channel, The Journal of Physiology, Vol 558, 417-431 (2004)

doi: 10.1113/jphysiol.2004.062588

[47] Wang S., Liu S., Morales M. J., Strauss H. C., Rasmusson R. L., A quantitative analysis of the activation and inactivation kinetics of HERG expressed in Xenopus oocytes, The Journal of Physiology, Vol 502, 45-60 (2004)

https://doi.org/10.1111/j.1469-7793.1997.045bl.x

[48] Hardman R. and Forsythe I., *Ether-a-go-go* ‘ -related gene K+ channels contribute to threshold excitability of mouse auditory brainstem neurons, The Journal of Physiology 587, 2487-2497 (2009)

[49] Wang J., Ou, Shao-Wu, Wang Yun-Jie, Distribution and function of voltage-gated sodium channels in the nervous system, Channels (Austin) 11, 534-554 (2017)

doi: 10.1080/19336950.2017.1380758

[50] Catterall W., Structure and function of voltage-gated Sodium Channels at Atomic Resolution, Experimental Physiology, Vol 99, 35-51 (2013)

[51] Payandeh J., Scheuer T., Zheng N., Catterall W., The crystal structure of a voltage-gated sodium channel, Nature 475, 353-358 (2011)

doi:10.1038/nature10238

[52] Hameed S., Nav1.7 and Nav1.8: Role in the pathophysiology of pain, Molecular Pain (2019)

doi: 10.1177/1744806919858801

[53] Vasylyev D., Han C. et al., Dynamic-clamp analysis of wild-type human Nav1.7 and erythromelalgia mutant channel L858H, Journal of Neurophysiology 111, 1429-1443 (2014)

doi:10.1152/jn.00763.2013

[54] Immonen E. V., French A. S., Torkkeli P. H. et al., EAG channels expressed in microvillar photoreceptors are unsuited to diurnal vision, Journal of Physiology, 5465-5479 (2017), doi: 10.1113/JP273612

[55] Perkins K. L., Cell-attached voltage-clamp and current-clamp recording stimulation techniques in brain slices, Journal of Neuroscience Methods, Vol. 154, 1-18 (2006)

https://doi.org/10.1016/j.jneumeth.2006.02.010